Gene Expression Patterns 9 (2009) 475–489

Contents lists available at ScienceDirect

Gene Expression Patterns

journal homepage: www.elsevier.com/locate/gep

Comparative analysis of conditional reporter alleles in the developing embryo and embryonic nervous system

Debra Ellisor [a], Dorothy Koveal [a], Nellwyn Hagan [b], Ashly Brown [b], Mark Zervas [a,*,1]

[a] Department of Molecular Biology, Cell Biology and Biochemistry, Division of Biology and Medicine, Brown University, 70 Ship St., Providence, RI 02903, USA
[b] Department of Neuroscience, Division of Biology and Medicine, Brown University, 70 Ship St., Providence, RI 02903, USA

ARTICLE INFO

Article history:
Received 26 September 2008
Received in revised form 9 July 2009
Accepted 10 July 2009
Available online 16 July 2009

Keywords:
En1^{Cre}
Wnt1-CreER^{T}
Cell lineage
Neural circuits
Midbrain
Spinal cord
Trigeminal ganglia
Conditional phenotyping alleles
Genetic Inducible Fate Mapping

ABSTRACT

A long-standing problem in development is understanding how progenitor cells transiently expressing genes contribute to complex anatomical and functional structures. In the developing nervous system an additional level of complexity arises when considering how cells of distinct lineages relate to newly established neural circuits. To address these problems, we used both cumulative marking with Cre/*loxP* and Genetic Inducible Fate Mapping (GIFM), which permanently and heritably marks small populations of progenitors and their descendants with fine temporal control using *CreER/loxP*. A key component used in both approaches is a conditional phenotyping allele that has the potential to be expressed in all cell types, but is quiescent because of a *loxP* flanked *Stop* sequence, which precedes a reporter allele. Upon recombination, the resulting phenotyping allele is 'turned on' and then constitutively expressed. Thus, the reporter functions as a high fidelity genetic lineage tracer *in vivo*. Currently there is an array of reporter alleles that can be used in marking strategies, but their recombination efficiency and applicability to a wide array of tissues has not been thoroughly described. To assess the recombination/marking potential of the reporters, we utilized *CreER*^{T} under the control of a *Wnt1* transgene (*Wnt1-CreER*^{T}) as well as a cumulative, non-inducible *En1*^{Cre} knock-in line in combination with three different reporters: *R26R* (LacZ reporter), *Z/EG* (EGFP reporter), and *Tau-Lox-STOP-Lox-mGFP-IRES-NLS-LacZ* (membrane-targeted GFP/nuclear LacZ reporter). We marked the *Wnt1* lineage using each of the three reporters at embryonic day (E) 8.5 followed by analysis at E10.0, E12.5, and in the adult. We also compared cumulative marking of cells with a history of *En1* expression at the same stages. We evaluated the reporters by whole-mount and section analysis and ascertained the strengths and weaknesses of each of the reporters. Comparative analysis with the reporters elucidated complexities of how the *Wnt1* and *En1* lineages contribute to developing embryos and to axonal projection patterns of neurons derived from these lineages.

1. Results and discussion

1.1. Cumulative marking and Genetic Inducible Fate Mapping (GIFM) methodology

Physical fate mapping methods have contributed substantially to understanding developmental mechanisms, but these approaches vary based on methodical procedures, are invasive, and do not provide information on the genetic history of physically marked cells (reviewed in Zervas et al., 2005). By comparison, gene expression analysis alone is not sufficient for following the fate of cells during development because many developmentally regulated genes are rapidly extinguished and gene expression patterns are dynamic in varying populations. For example, the transcription factor *Engrailed 1* (*En1*), which is expressed in the primordia of the Mb (mesencephalon, mes) and Cb (rhombomere 1, r1) is progressively restricted between E8.5 and E12.5 (Fig. 1A–D) (reviewed in Zervas et al., 2005). *En1* is also expressed in the dermatome and proximal mesenchyme, costal precursors, limb bud ectoderm, and in the ventral spinal cord (SC) (Davidson et al., 1988). The secreted signaling molecule *wingless-related MMTV integration site 1* (*Wnt1*), which is broadly expressed in the mes and migrating neural crest at E8.5, is dynamically regulated between E8.5 and E9.5 to become more restricted in the mes (reviewed in Zervas et al., 2005) and is also expressed in the posterior Hb and dorsal SC (Fig. 1E–H) (Wilkinson et al., 1987). While northern blot analysis and *in situ* hybridization (ISH) provide a snapshot of *En1* and *Wnt1* gene expression patterns (Davidson et al., 1988; Joyner and Martin, 1987; Wilkinson et al., 1987), they are insufficient to reveal how cells expressing these genes contribute to developing and mature tissues.

* Corresponding author. Address: Laboratory of Developmental Neurobiology, Genetics and Neurological Disease, Department of Molecular Biology, Cell Biology and Biochemistry, Division of Biology and Medicine, Box G-E436, Brown University Providence, RI 02912, USA. Tel.: +1 401 863 6840; fax: +1 401 863 9653.
E-mail address: Mark_Zervas@brown.edu (M. Zervas).
URL: http://research.brown.edu/myresearch/Mark_Zervas (M. Zervas).
[1] Present address: Laboratories for Molecular Medicine, 70 Ship Street, Rm. 436, Providence, RI 02903, USA.

1567-133X/$ - see front matter © 2009 Elsevier B.V. All rights reserved.
doi:10.1016/j.gep.2009.07.007

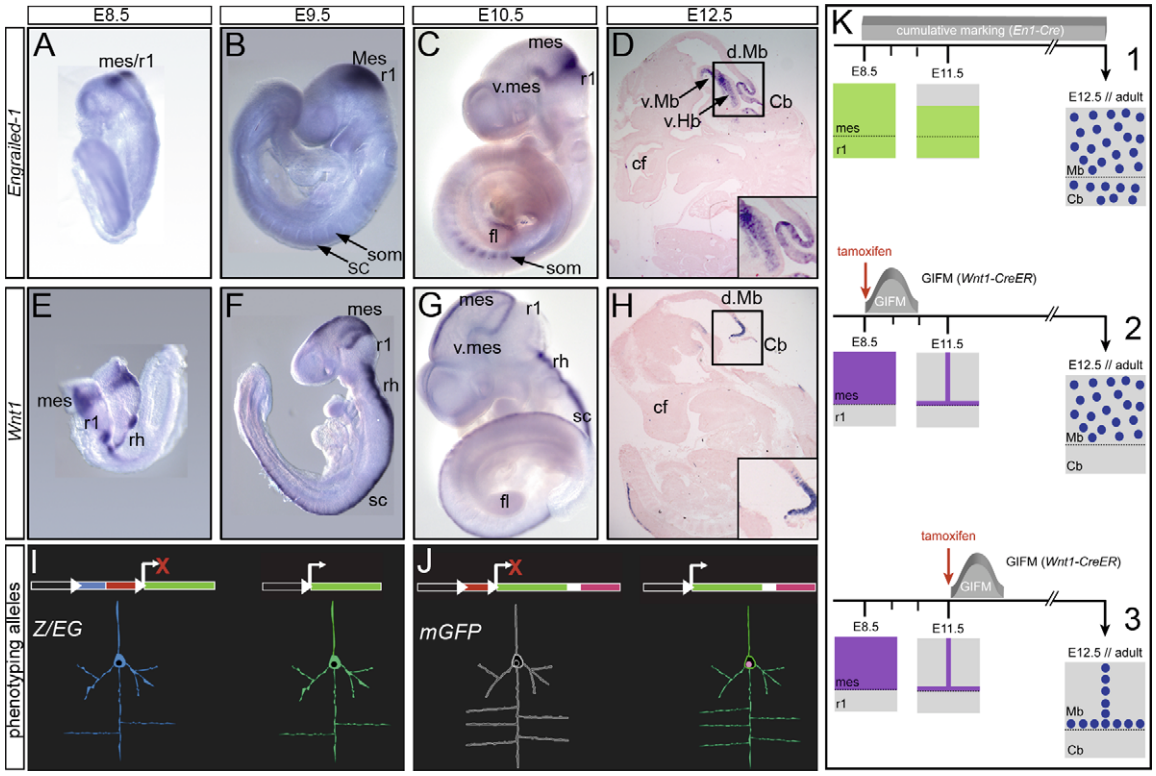

Fig. 1. *En1* and *Wnt1* gene expression domains and genetic marking approaches. *En1* is expressed in the mes/r1 at E8.5 (A). By E9.5 the mes/r1 domain expands with *En1* localized to the entire mes (B). At E10.5 *En1* is restricted to the posterior mes and in r1 as well as in somites (som) and forelimb (fl) (C). *En1* at E12.5 is localized to the inferior colliculus of the dorsal midbrain (d. Mb), the cerebellum (Cb), and spans the ventral Mb (v. Mb) and ventral–anterior hindbrain (v. Hb); note the lack of expression in craniofacial (cf) regions (D). *Wnt1* is expressed in the mes at the open neural tube stage (E8.5) and in more posterior rhombomeres (rh); note the lack of expression in r1 (E). After neural tube closure, *Wnt1* becomes restricted to the midline of the dorsal and ventral mes and to a ring at the posterior mes; *Wnt1* is also expressed in posterior rh and in the spinal cord (SC) (F, G). By E12.5, *Wnt1* is detected in the inferior colliculus of the d. Mb (H) and faintly in the caudal part of the embryo. These expression patterns reveal the domains that will be marked cumulatively by $En1^{Cre}$ or temporally by tamoxifen administration at E8.5 by *Wnt1-CreER*^{T}. The *Z/EG* (I) and *mGFP* (J) phenotyping alleles are shown in schematic form. Prior to recombination cells expressing the *Z/EG* allele can be detected by β-galactosidase (β-gal) activity or expression (blue), but cells that have undergone recombination can be detected by EGFP fluorescence or GFP immunolabeling (I, green). In contrast, unrecombined cells in *mGFP* mice are not marked (J), but after recombination, "marked" cells are detected by either GFP (green) or nuclear β-gal (red) immunocytochemistry (J). Schematic illustrations of cumulative marking (K-1) and GIFM (K-2, K-3) strategies. Illustrations of the *En1* and *Wnt1* gene expression domains in the mes/r1 during early embryogenesis are shown as examples below the time line. The stages where marking occurs are indicated above the time line and the ensuing, marked domains are assessed as described in the text.

It is possible to overcome these limitations using genetic methods (for example *Cre/loxP* technology), which forge a link between gene expression, cell behaviors, and the ultimate fate of cells (Dymecki and Kim, 2007; Joyner and Zervas, 2006). Cre recombinase (Cre) and conditional (*loxP-Stop-loxP)* phenotyping alleles (Fig. 1I, J) allow for the cumulative marking of cells in a tissue- or cell-type specific manner (Zinyk et al., 1998). The selectivity of marking is achieved by using gene regulatory elements to control the expression of Cre in genetically-defined domains (Supplemental Fig. 1). Cre recognizes *loxP* sequences and mediates recombination in a site-specific manner, which results in the deletion of intervening sequences when the *loxP* sites are in the same orientation. In this system, Cre-mediated recombination occurs as long as the gene that is controlling Cre is expressed (Fig. 1K-1).

In contrast, GIFM allows progenitors of a defined genetic lineage to undergo recombination with both spatial and temporal control (Joyner and Zervas, 2006) (Fig. 1K-2, K-3). Cells, having undergone recombination, are essentially uncoupled from gene expression and are permanently marked. The marked cells and their descendants can then be tracked at varying stages of development and can be detected in their final position in the adult (Dymecki and Kim, 2007; Joyner and Zervas, 2006; Zervas et al., 2005). GIFM is a tripartite system that uses the following components: *Cre* that is fused with a mutated estrogen receptor ligand binding domain (*CreER*^{T}), a conditional *loxP-Stop-loxP* phenotyping allele, and tamoxifen. The *CreER*^{T} modification ensures that Cre is sequestered in the cytoplasm by heat shock protein 90 (Hsp90) (Feil et al., 1996). Spatial control of *CreER*^{T}, and therefore recombination, is achieved by placing *CreER*^{T} under the control of gene regulatory elements. Tamoxifen, which takes approximately 6 h to enter the embryo, binds to ER and releases CreER^{T} from Hsp90. Subsequently, CreER^{T} enters the nucleus where recombination occurs (Feil et al., 1996; Hayashi and McMahon, 2002; Robinson et al., 1991; Zervas et al., 2004). Thus, tamoxifen administration confers temporal control of when recombination is initiated while tamoxifen pharmacokinetics ensures that *CreER*^{T} release, and therefore recombination, happens for 30 h (Robinson et al., 1991) (Fig. 1K-2, K-3). *CreER*^{T} plus tamoxifen concomitant with the presence of a conditional phenotyping allele causes the removal of the *loxP* flanked *Stop* sequence and brings the reporter of the phenotyping allele under the control of a constitutive promoter.

The most commonly used conditional reporter line of mice is the *R26R* line (Soriano, 1999), which consists of *loxP-Stop-loxP-LacZ*, and when recombined allows *LacZ* to be expressed and β-galactosidase (β-gal) to be produced (Soriano, 1999). This line has been utilized with an array of *CreER* driver lines in GIFM experiments to ascertain how the midbrain (Mb), cerebellum (Cb), and limb develop as well as to determine the presence of adult neural stem cells *in vivo* (Kimmel et al., 2000; Guo et al., 2003; Zervas et al., 2004; Ahn and Joyner, 2004, 2005). Additional reporters

are the green *f*luorescent *p*rotein (GFP) phenotyping alleles, *Z/EG* and *mGFP* (Fig. 1I, J). The *Z/EG* allele is comprised of a *loxP* flanked β-geo (*LacZ-neomycin*) stop cassette upstream to *GFP* (Fig. 1I). In the absence of Cre, cells express β-gal, but after recombination, *LacZ* is deleted and *GFP* comes under the control of the chick beta-actin promoter (Novak et al., 2000). The *mGFP* allele utilizes the *Tau* promoter to drive a *loxP* flanked *Stop* cassette and a 3′ modified *membraneGFP-IRES-nuclearLacZ* allele (Fig. 1J). In the absence of Cre, cells are unmarked. Cre-mediated recombination allows a bi-cistronic message of *mGFP-IRES-nLacZ* to independently produce β-gal, which is localized to the nucleus, and mGFP, which is enriched in axons (Hippenmeyer et al., 2005). A comprehensive comparison delineating the strengths and research value of these reporters has not been undertaken. In particular, the *Z/EG* (Novak et al., 2000) and *mGFP* (Hippenmeyer et al., 2005) reporter lines have not been evaluated side by side and in relation to the *R26R* line in a detailed multi-tissue and lineage-specific manner. In this report, we use three different phenotyping alleles in combination with $En1^{Cre}$ and $Wnt1\text{-}CreER^{T}$ mice to assess the recombination patterns in these reporter lines.

We fist compared *En1* or *Wnt1* expression to *Cre* expression by ISH to confirm that *Cre*, and therefore marking, would faithfully occur in appropriate domains (Supplemental Fig. 1). Cumulatively marked domains in sections from $En1^{Cre}$ embryos were compared to adjacent sections labeled with *En1* and *Cre* probes (Supplemental Fig. 1A–J). Cells in the posterior Mb and Cb expressed *En1* and *Cre* at E12.5 in domains that were similar to the regions observed with genetic marking (Supplemental Fig. 1C–E). Notably, neither *En1* nor *Cre* were expressed in the trigeminal ganglia (Supplemental Fig. 1F–J). We also compared domains conditionally marked with $Wnt1\text{-}CreER^{T}$ and tamoxifen administration at embryonic day (E)8.5 to adjacent sections labeled with *Wnt1* and *Cre* probes (Supplemental Fig. 1K–T). At E12.5, both *Wnt1* and *Cre* were expressed in similar domains in the Mb (Supplemental Fig. 1K–O) and lateral posterior Hb (Supplemental Fig. 1P–Q), but neither were expressed in the trigeminal ganglia (Supplemental Fig. 1P–T). Because of the overlapping and segregated expression domains (Fig. 1), we directly compared similar regions (e.g. dorsal and ventral Mb) in cumulative and conditional marking conditions. We also took advantage of $En1^{cre}$ and $Wnt1\text{-}CreER^{T}$ mice to ascertain developmental aspects of different tissues in which marking has occurred.

1.2. Cumulative marking with $En1^{Cre}$ and R26R, Z/EG, and mGFP phenotyping alleles

We initially assessed mouse embryos at E12.5 because at this stage most tissues are comprised of both proliferating progenitors and newly differentiated cells. In addition, immature neural circuits are forming in the nervous system.

The *R26R* reporter allele is widely expressed throughout development and in the adult (Soriano, 1999). $En1^{Cre}$;*R26R* embryos processed by whole-mount x-gal labeling (4 h) revealed that cells with a history of expressing *En1* reside in the entire dorsal and ventral Mb, Cb, ventral SC, and intercostal regions as well as in limb buds and craniofacial domains (Fig. 2A–D). The *Z/EG* reporter is also expressed in numerous domains, with different levels of marking occurring in a tissue-specific manner (Novak et al., 2000; Guo et al., 2002), which may depend on the promoter driving this transgene or the transgene site of integration in the genome. Marked (GFP+) domains in $En1^{Cre}$;*Z/EG* embryos at E12.5 were readily detected by whole-mount fluorescent imaging (Fig. 2E–H). The *Z/EG* reporter revealed marked cells in the dorsal and ventral Mb, Cb, ventral SC, limb buds, and in the body wall lateral to the SC (Fig. 2E–H). Unlike with the *R26R* reporter, we could not detect marking in intercostal regions in whole-mount preparations with the *Z/EG* reporter (compare Fig. 2A and E). In contrast to the *R26R* reporter, faintly labeled axonal projections (GFP+) with the *Z/EG* reporter could be observed in craniofacial structures (Fig. 2E, inset) and could also be seen emanating from the SC (Fig. 2H, inset). Labeling in $En1^{Cre}$;*mGFP* embryos at E12.5 (Fig. 2I–L) appeared substantially different from either $En1^{Cre}$;*R26R* or $En1^{Cre}$;*Z/EG* embryos. First, labeling was only seen in a subset of the Mb and Cb, as compared to *R26R* and *Z/EG* (see Fig. 2A, C, E, G, I and K). In addition, stronger labeling was observed in the SC, but was not detected in the body wall (compare Fig. 2A, D, E, H, I and L). Other differences included an absence of labeling in the limb bud (see Fig. 2I versus E) and very prominent labeling of neuronal projections and vibrissae in the craniofacial area (see Fig. 2J versus F). Collectively, whole-mount analysis revealed numerous similarities in the distribution of cell somata that were marked using the *R26R* and *Z/EG* phenotyping alleles while the *mGFP* reporter appeared to primarily label neuronal populations and produced GFP that was enriched in axonal projections (Fig. 2).

While whole-mount analysis is valuable for the 3-dimensional determination of spatial domains derived from marked cells and for the observation of axonal projections, the relative sensitivity of the detection method for each reporter confounds a direct comparison between the lines. In addition, whole-mount labeling does not allow for detailed cellular or cytoarchitectural analysis. Therefore, we sectioned cryoprotected embryos and processed them for either β-gal or GFP immunolabeling. Recombined (marked) cells in E12.5 $En1^{Cre}$;*R26R* embryos were detected by β-gal immunocytochemistry labeling (Fig. 3). The cellular distribution of marked cells recapitulated the findings in whole-mount preparations. There was an abundance of labeled cells in the Mb, Cb, ventral Hb (Fig. 3A–D), SC, and intercostal domains (data not shown). Marked cells were also observed in craniofacial tissue that was adjacent to the more posteriorly positioned and labeled trigeminal ganglia (Fig. 3E). Marked cells overlapped with dopamine neurons in the ventral Mb as previously described (Fig. 3C) (Zervas et al., 2004).

In a complementary manner, E12.5 $En1^{Cre}$;*Z/EG* embryos showed marked (GFP+) cell bodies in the dorsal and ventral Mb as well as in the Cb and v. Hb (Fig. 4A–D). In contrast to the *R26R* reporter, the *Z/EG* phenotyping allele allowed us to observe axonal projections of marked cells due to GFP distribution throughout the cell. In the ventral Mb, cells were distributed throughout the entire domain spanning the ventricular zone to the mesencephalic flexure and projections appeared to be located proximal to the flexure (Fig. 4C). To enhance our understanding of the projection patterns of cells with a history of expressing *En1*, we analyzed transverse sections obtained from various dorsal–ventral locations (Fig. 4G). In the dorsal Mb, axons were intermingled and difficult to discriminate amongst marked cells (Fig. 4G-1). This was also true in the ventral Mb (Fig. 4G-2). At the level of the Cb, a bundle of axons was observed to emanate caudally, consistent with sagittal sections (data not shown). We also observed $En1^{Cre}$;*Z/EG* marked cells and projections in the trigeminal ganglia (Fig. 4E and F) and distributed throughout craniofacial tissue (Fig. 4F, data not shown). ISH with an anti-sense *En1* probe showed that *En1* gene expression was not detected in the trigeminal ganglia or in craniofacial tissue (Fig. 1D, Supplemental Fig. 1F–J) suggesting that the *En1*-derived cells were derived from migrating neural crest at an earlier stage of development.

In sagittal sections from $En1^{Cre}$;*Z/EG* embryos, we observed axons emanating from the dorsolateral anterior Hb (Fig. 4E), which coursed toward the trigeminal ganglia (Fig. 4E and F). The projections de-fasciculated at an anterior point with a portion of the projections extending into the trigeminal ganglia and the remaining axons coursing caudally in a conduit that traverses the entire length of the Hb to the SC (Fig. 4E, arrows). In contrast, the ventromedial anterior Hb, which had marked cells confined to this do-

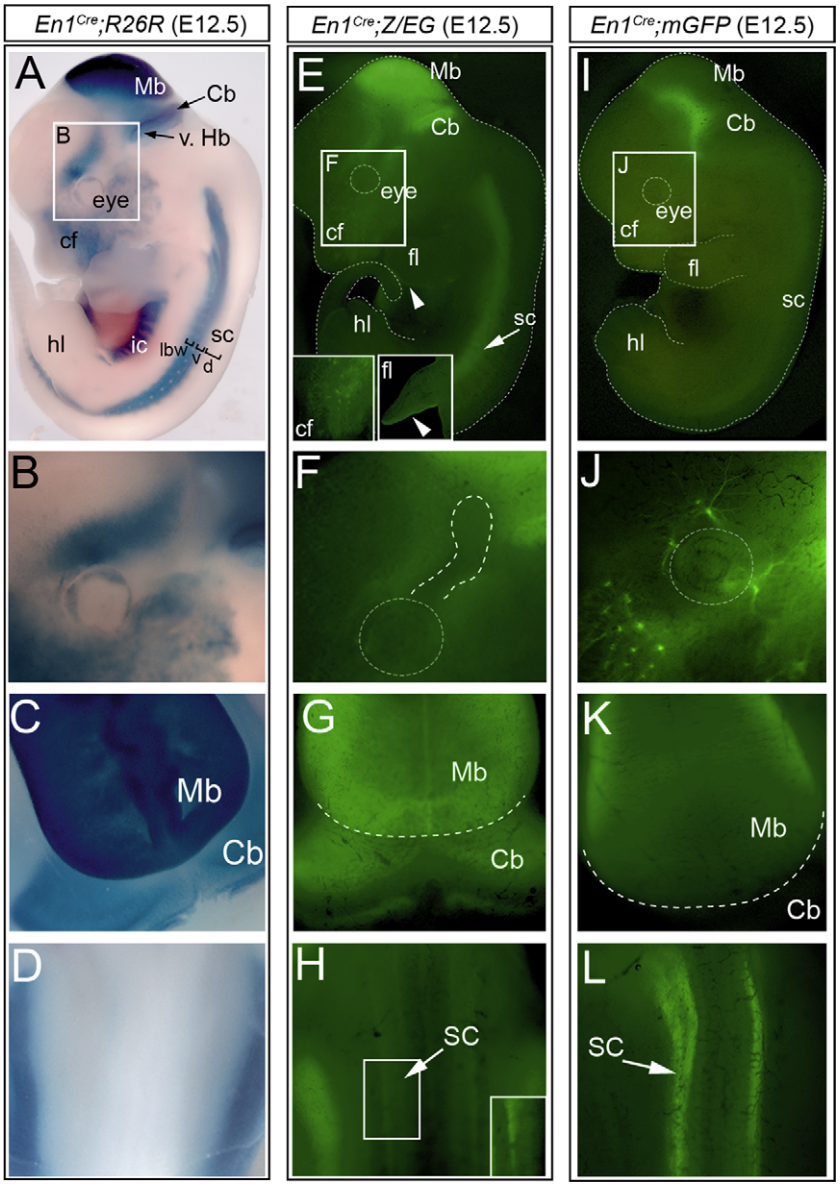

Fig. 2. Cumulative marking of cells with a history of expressing *En1* in E12.5 embryos. At E12.5, cumulatively marked *En1*-expressing cells in *En1*^{Cre}*;R26R* embryos were detected by whole-mount x-gal labeling (for 4 h) (A–D). Cells with a history of *En1* expression populated the entire Mb, Cb and ventral–anterior Hb (v. Hb) (A, C). Craniofacial (cf) structures surrounding the eyes were also clearly visible (A, B). The intercostal domain (ic), the lateral body wall (lbw), and putative ventral SC were prominently marked (A, D); marking of the limbs (fl and hl) was not visible because of the angle and faint labeling. Marked cells in *En1*^{Cre}*;Z/EG* embryos could be detected by endogenous fluorescence on a fluorescent dissecting scope (E–H) and the marked pattern was similar to *En1*^{Cre}*;R26R* mice. Also, the ventral domains of the forelimb (fl) and hindlimb (hl) were labeled (E, arrowhead; inset). Marked cells were prominent in the craniofacial region (cf) and could be seen in the vicinity of the vibrissae (E, inset). In addition, two thick cohorts of GFP+ cells were located posteriorly on the dorsal and ventral side of the eye juxtaposed between the eye and the ventral Mb/Hb (F). The entire Mb (E, G) and the full extent of the Cb (G) as well as the lateral body wall (E) were labeled. There was also a faint bundle of labeled axons in the putative ventral SC (H, arrows, inset). Notably, we could not readily detect the SC in sagittal views nor could we detect intercostal domains that were observable by whole-mount in *En1*^{Cre}*;R26R* mice. The cf and sc insets in E and H are from regions indicated by marquees that were subject to increased brightness and contrast adjustments to more clearly show the structures. The fl inset is from a coronal view of the same embryo to better view limb labeling. *En1*^{Cre}*;mGFP* embryos (I–L) were densely labeled in the ventral Mb (v. Mb) while fine radially oriented projections were seen in the dorsal Mb (I, K). Labeling was not visible in the Cb, likely due to a small number of differentiating neurons revealed with the *mGFP* reporter. Within the craniofacial (cf) domain, there was invariant labeling around the eye and also dispersed as distinct puncta in close proximity to the vibrissae (J). A distinct bilateral set of marked cells/projections was located in the dorsal SC (L, arrow). Non-neural domains including the limbs (fl and hl), intercostal domains and lateral body wall were unmarked.

main by a posterior lineage boundary (Fig. 4D, arrowheads) (Zervas et al., 2004), had a broad swath of axons projecting from the marked domain to more caudal regions (Fig. 4D, bracket). A bilateral cluster of marked neurons was also prominently labeled in the ventral SC (Fig. 4G-3, arrow) with peripherally oriented axons (Fig. 4G-3, brackets). An additional lateral population of *En1-Cre* marked cells was located in distinct bands in the lateral body wall (Fig. 4G-3).

We next assessed cells marked with *En1*^{Cre} and the *mGFP* allele at the cellular level (Fig. 5). An advantage of the *mGFP* allele is that we were able to detect marked cells with clarity because of strong nuclear β-gal expression, while mGFP expression was faintly, but reliably detected in cell bodies, and robustly present in axonal projections (Fig. 5A). In the dorsal Mb and in the Cb we detected small cohorts of β-gal+ cells organized into a narrow zone distal from the ventricle (Fig. 5B), which were apparently differentiating neurons

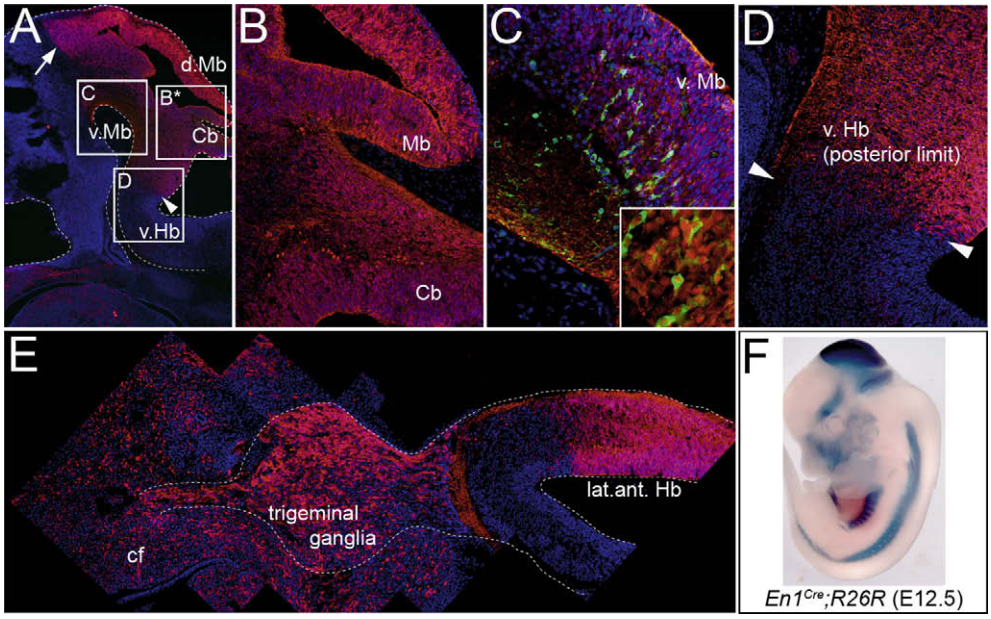

Fig. 3. Cellular analysis of cumulative marking in E12.5 *En1^{Cre};R26R* embryos. Sagittal sections were immunolabeled with an anti-β-gal antibody to detect Cre-mediated recombination in *En1* derived cells (red) and counter stained with the nuclear marker Hoechst 33342 (blue) (A–E). The entire Mb, Cb, and ventral Hb were marked (A–D). Marked cells in the ventral Mb contributed to maturing tyrosine hydroxylase (TH)+ dopamine neurons (C). A sharp line of demarcation delineated the anterior limit of the Mb (A, arrow) and the posterior limit of the ventral–anterior Hb (A, D, arrowheads). The asterisk (B*) in A indicates that the section shown at high magnification in B was from an adjacent section with higher tissue quality. Laterally, trigeminal ganglia were comprised of marked cells (E). Cells in the lateral–anterior Hb were marked and a bundle of labeled projections coursed toward the trigeminal ganglia at the Hb flexure (E). *En1^{Cre}* marked cells also densely populated the rostral craniofacial (cf) region (E). A whole-mount view of the embryo is shown (F).

located in a well-defined differentiated zone (DZ) (Fig. 5B). In contrast, *R26R* and *Z/EG* marked both differentiating cells and progenitors in the ventricular zone (VZ) (Figs. 3 and 4B). This was confirmed by comparing the genetically marked cells with phosphorylated histone H3 (pHH3) immunolabeling, which indicates mitotic cells (Fig. 6). Marked cells in *En1^{Cre};mGFP* embryos were not located in the proliferating pHH3+ VZ, but were positioned in the DZ in the Mb and Cb (Fig. 6A, B and H). In contrast, the *En1* lineage marked in *En1^{Cre};R26R* and *En1^{Cre};Z/EG* embryos showed overlap with pHH3 in these regions (Fig. 6I and J). *En1^{Cre};mGFP* marked neurons located adjacent to the periphery of the dorsal Mb had short projections that extended toward the surface (Fig. 5B, inset). Transverse sections (planes shown in Fig. 5G) processed for β-gal/GFP double immunocytochemistry revealed that *En1*-derived cells of the dorsal Mb consisted of a small peripheral cluster of differentiating neurons that largely sent axons in a peripheral and rostral location (Fig. 5G-1). In the ventral Mb, the β-gal+ differentiating neurons (Fig. 5C, DZ) were co-localized with marked (GFP+) axons (Fig. 5C). Transverse sections revealed that the ventral Mb contained two bilateral clusters of marked neurons that had a complex projection pattern with axons that moved radially outward (Fig. 5G-2, arrowheads) although there was a conduit of axons that crossed the midline (Fig. 5G-2, bracket).

By directly comparing the ventromedial anterior Hb using the *Z/EG* versus *mGFP* alleles, we observed that marked cells that are confined to r1 by a well-defined posterior lineage boundary (Fig. 5D, arrowheads) (Zervas et al., 2004), have caudally oriented axons (Fig. 5D, bracket versus 4D, bracket). Similarly, cumulatively marked cells of the lateral Hb were distributed throughout the DZ in the dorsal half of the lateral Hb and did not extend past a sharp border located dorsal to the flexure (Fig. 5F, yellow arrow). Projections from the lateral Hb coursed superficially where they then extended in a caudal direction (Fig. 5E, arrows). Upon closer inspection, this axonal bundle could be partitioned into multiple projection pathways including a deep, broad zone of caudally oriented projections, a dense superficial conduit, and a thick fascicle at the flexure of the Hb that connected with the trigeminal ganglia (Fig. 5F, see Section 1.4, Neural Projections for details). *En1*-derived neurons of the trigeminal ganglia were β-gal+/GFP+ (Fig. 5F) and innervated the rostral craniofacial region (Fig. 5F). The marked cells in the trigeminal ganglia did not express *En1* transcripts at E12.5 (Supplemental Fig. 1F–J) and were not mitotic based on the complete absence of pHH3 immunolabeling in all three reporter lines (Fig. 6E–G). This is the first report that we are aware of describing the contribution of the *En1* lineage to the trigeminal ganglia. In contrast to *En1^{Cre};Z/EG* and *En1^{Cre};R26R* lines, which had marked cell bodies in the craniofacial regions, *En1^{Cre};mGFP* embryos did not have marked somata in rostral craniofacial tissue suggesting that the *En1*-derived cells in the craniofacial region were not differentiated neurons. In sagittal sections of SC, a ventral band of cells was observed that extended fine axonal processes ventrally to form a thick bundle of axons (data not shown). Transverse sections through the SC confirmed that the band of marked cells in sagittal sections was indeed two bilateral clusters of marked cells localized to the ventral–lateral SC (Fig. 5G-3). Unlike in *En1^{Cre};Z/EG* embryos, marked cells in E12.5 *En1^{Cre};mGFP* mice were not observed in the body wall adjacent to the SC (Fig. 5G-3 versus 4G-3).

In summary, both the *R26R* and *Z/EG* reporters revealed a similar profile of marked cells that had a history of expressing *En1*, which consisted of both proliferating and differentiating cells. The *mGFP* reporter allele yielded extremely bright labeling of neuronal processes and axonal trajectories by whole-mount epi-fluorescence at E12.5 with cumulative marking although cell somata were more difficult to observe at this level because GFP is not heavily distributed in cell bodies. We were unable to detect non-neural tissues with the *mGFP* reporter, likely because the promoter *Tau*, under which this *GFP* allele is controlled, is enriched in the nervous system (Aronov et al., 2001; Hashimoto et al., 2008).

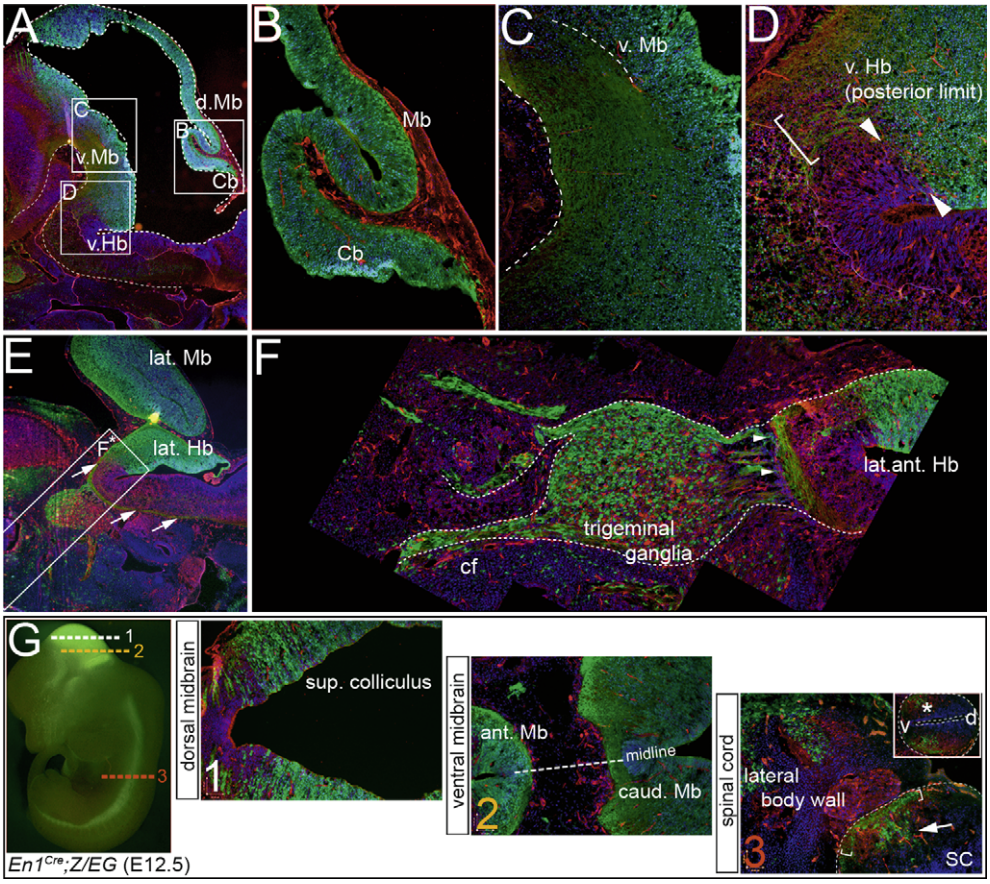

Fig. 4. Cellular analysis of cumulative marking in E12.5 *En1^{Cre};Z/EG* embryos. Sagittal sections were double immunolabeled with antibodies recognizing β-gal (un-recombined cells, red) and GFP (recombined "marked" cells, green) and counter stained with the nuclear marker Hoechst 33342 (blue) (A–F). The dorsal Mb both medially (A, B) and laterally (E) was marked nearly in its entirety. There were unlabeled cells primarily in the most rostral–medial Mb (A) and in the more dorsal–lateral (Mb) (E). The posterior Mb and the Cb were densely populated with cells marked with *En1^{Cre}* (B). The ventral Mb was composed of densely marked cells as well as axonal projections, but the extent of their marking prohibited a clear demarcation between cell bodies and axons (C). A sharp boundary of marked cells was seen at the posterior limit of the ventral Hb (D, arrowheads), consistent with the *R26R* reporter. We also observed axonal projections emanating posteriorly from the v. Hb (D, bracket), which then traversed the ventral half of the brainstem. GFP+ cells filled the lateral–anterior Hb (E, arrows) with a tight bundle of axons that coursed ventrally along the ventral surface (E). Notably, this bundle was much tighter and ran along a narrower trajectory versus the bundles that arose from the medial anterior Hb (compare D–E). At the point of the putative pontine flexure, a group of axons bifurcated from the main bundle and formed a contiguous network with the trigeminal ganglia and more rostral craniofacial tissue (E, F; arrowheads). To more fully discern the marked populations, we also assayed transverse sections (obtained from planes shown in G): Cells with a history of expressing *En1* were radially organized and completely spanned the neuroepithelial tissue in the dorsal Mb (G-1) and the ventral Mb (G-2). In the SC, a bilateral cluster of GFP+ cells was located in the ventral–lateral cord (G-3, arrow) and clearly sent axons toward the cord periphery (G-3, brackets) where they formed a fascicle that exited the cord. Marked cells were also seen lateral to the SC in the body wall and intercostal domains (G-3). The inset in G-3 shows a low magnification view of the entire SC while G-3 shows half of the SC and a portion of the lateral body wall.

1.3. GIFM with Wnt1-CreER^T and R26R, Z/EG, and mGFP phenotyping alleles

We next tested the three reporter alleles in a GIFM experimental paradigm by breeding *Wnt1-CreER^T* males also carrying our reporter alleles (*Wnt1-CreER^T;R26R*, *Wnt1-CreER^T;mGFP*, *or Wnt1-CreER^T;Z/*EG) to Swiss Webster (wildtype) females and delivered tamoxifen by oral gavage to pregnant females carrying embryos at E8.5. We used our well-characterized *Wnt1-CreER^T* mice because of the ability to elicit recombination in a wide array of tissue/cell types when tamoxifen is administered at E8.5 (Zervas et al., 2004). Tamoxifen pharmacokinetics confer that recombination occurs during a peak period of 12–24 h after administration, following a 6 h delay while tamoxifen enters the uterus (Robinson et al., 1991). We also took advantage of transient (*Wnt1-CreER^T*) versus cumulative (*En1^{Cre}*) marking to ascertain how these two lineages contributed to neural crest, Mb, and SC at E12.5. *Wnt1-CreER^T;R26R* embryos marked by tamoxifen administration at E8.5 were analyzed by whole-mount embryo x-gal labeling and by β-gal immunocytochemistry on sections at E12.5 (Fig. 7). *Wnt1*-derived cells were detected in the Mb, choroid plexus, the dorsal Hb posterior to the Cb and in the SC (Fig. 7A). The *Wnt1*-derived cells in the SC appeared to be localized dorsally to the cells cumulatively marked in *En1^{Cre};R26R* embryos (compare Figs. 7A versus 2A). Control embryos (*R26R plus* tamoxifen or *Wnt1-CreER^T;R26R without* tamoxifen) processed in x-gal were devoid of marking (Fig. 7A, inset; data not shown). In sections through the dorsal Mb, cohorts of cells were organized into linear clusters and had the appearance of clonally related cells (Fig. 7B). This organization was unique to medial/near-midline regions because neither dorsal–lateral Mb nor other tissue showed this same pattern (data not shown). While whole-mount x-gal labeling showed only faint labeling of craniofacial structures (Fig. 7A), section analysis revealed labeling through the craniofacial region (data not shown) and the trigeminal ganglia (Fig. 7C). In the SC, β-gal+ cells were localized to the dorsal root ganglia (DRG) (Fig. 7D).

In contrast to *Wnt1-CreER^T;R26R* embryos, we could not detect marked cells by whole-mount GFP fluorescence in *Wnt1-CreER^T;Z/EG* embryos at E12.5 (Fig. 8A). However, in sections from *Wnt1-CreER^T;Z/EG* embryos we could sporadically detect GFP+

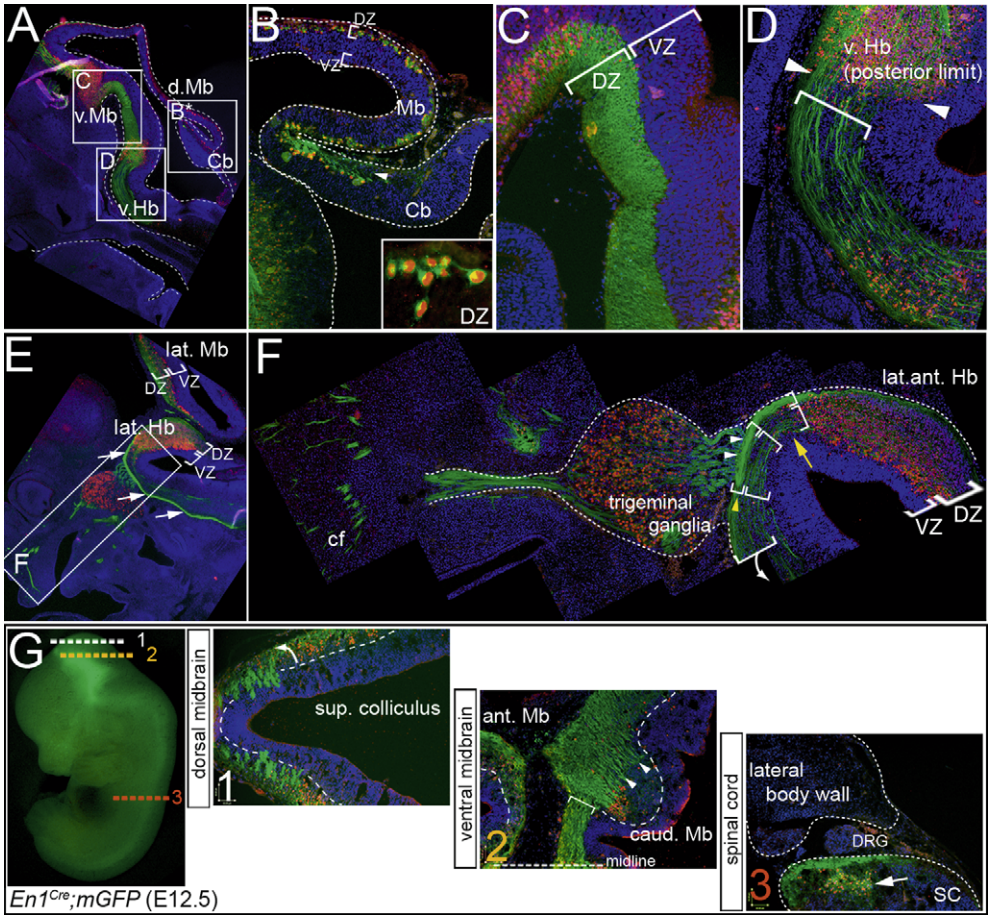

Fig. 5. Cellular analysis of cumulatively marked neurons and developing neural circuits in E12.5 *En1*^{Cre};*mGFP* embryos. Upon Cre mediated recombination, marked cells are detectable by nuclear β-gal labeling (red) and robust GFP labeling (green) of neuronal processes and faintly labeled soma. At low magnification the dorsal–medial and dorsal–lateral Mb and Cb of *En1*^{Cre};*mGFP* embryos appeared to be devoid of labeling (A). However, at high magnification marked cells were observed distal to the ventricular zone consistent with differentiating neurons (B, inset). The nuclei of marked cells formed a single DZ at the periphery of the dorsal Mb and in the Cb (B, arrowhead). In addition, fine projections radiated toward, and coursed along the surface of the Mb. In the Cb, axons emanated away from the DZ (B, arrowhead). The ventral Mb has β-gal+ nuclei and GFP+ processes that delineated differentiating neurons that had projections confined to DZ (C). *En1*-derived neurons of ventral–anterior Hb were organized into discrete clusters of differentiated neurons confined to the Hb by a posterior boundary (D, arrowheads). The Hb neurons had projections that emanated posteriorly and contributed to a conduit of axons that occupied the ventral half of the brainstem (D, bracket). Marked neurons (β-gal+) were distributed along the upper and anterior portion of the lateral Hb, but their projections emanated caudally (E, arrows). Projections bifurcated at the pontine flexure (I, white arrowheads) and formed a network with marked trigeminal ganglia neurons – axon bundles intermittently but stereotypically innervated the vibrissae of the anterior craniofacial domain (E, F). Other projections from the Hb coursed caudally (F, yellow arrowhead, arrow). In transverse sections obtained along the anterior–posterior axis (G), we observed differentiating neurons with projections that coalesced at the midline in a peripheral zone in the dorsal Mb (G-1). Neurons (β-gal+, red) were organized into discrete clusters in the ventral Mb (G-2). In the Mb, axons projected radially away from the marked neurons (G-2, white arrowheads) and joined a fascicle of axons crossing the midline (G-2, bracket). In the SC, cells with a history of expressing *En1* (β-gal+, red) were localized to the ventral–lateral cord (G-3, arrow) and their axons joined to form a fascicle at the periphery of the cord (G-3, bracket); note the lack of marked cells in the lateral body wall or intercostal domains that were marked with the *Z/EG* allele (compare 5G-3 to 4G-3).

cells, and although marked cells were sparse, they were located in the Mb (Fig. 8B and E), posterior Hb (Fig. 8C), and DRG (Fig. 8D) consistent with *Wnt1-CreER*^{T};*R26R* tissue. Thus, the relatively few marked cells with the *Z/EG* reporter allowed for unambiguous and detailed cellular morphology to be discerned (Fig. 8B–E).

Whole-mount analysis of *Wnt1-CreER*^{T};*mGFP* embryos at E12.5 revealed distinctly marked domains including the Mb, posterior Hb, and SC (Fig. 9A and B). In *Wnt1-CreER*^{T};*mGFP* embryos, the dorsal Mb contained sparse, radially organized projections (Fig. 9D) that were predominantly located at the lateral edges of the Mb (Fig. 9E, arrows). In contrast, a dense plexus was observed in the ventral Mb (Fig. 9D). A tight fascicle of axons was also observed in the caudal Hb (posterior to the Cb), and in the presumptive dorsal SC (Fig. 9B and F). Interestingly, projections from the upper SC coursed laterally and innervated the body wall and proximal forelimb (Fig. 9A, inset; 9C). We validated the marked population by immunocytochemistry on sections with antibodies recognizing β-gal and GFP. Section analysis of the dorsal Mb revealed that differentiating neurons with elaborate morphology formed a superficial zone with their projections radiating outward toward the surface (Fig. 9G). The *Wnt1* lineage also gave rise to neurons in the ventral Mb (Fig. 9H). Notably, β-gal+ cells (nuclei) were clustered together distally from the ventricle and had short projections that joined a dense plexus of projections, coursing both rostrally and caudally at the ventral mes flexure (Fig. 9H) suggesting that differentiating neurons were formed into distinct ventral nuclei similar to the organization of the adult ventral Mb (Paxinos, 2004). *Wnt1*-derived neurons also had axons in the ventral third of the posterior Hb (Fig. 9I). The *Wnt1*-derived neurons marked at E8.5 in the trigeminal ganglia were largely bipolar (Fig. 9J). This example is the first that we are aware of describing the temporal contribution of the *Wnt1* lineage to the trigeminal ganglia. These observations coupled with the similar distribution and pattern of axonal projections as seen in cumulatively marked *En1*^{Cre};*mGFP* embryos (compare Fig. 9J to Fig. 5E and F) strongly suggest that *En1* and *Wnt1* derived neural crest cells contribute to similar craniofacial structures.

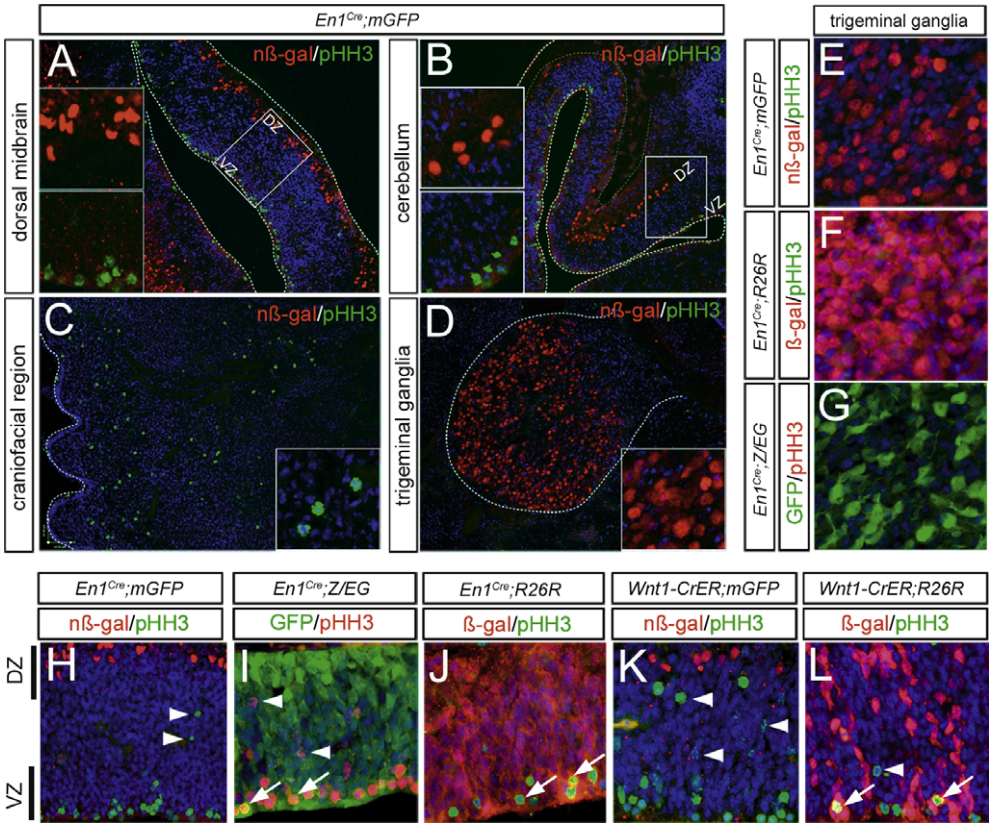

Fig. 6. The *mGFP* reporter is expressed in differentiated neurons while *R26R* and *Z/EG* are expressed in both differentiated neurons and proliferating progenitors. The Mb, Cb, craniofacial region, and trigeminal ganglia were evaluated in E12.5 *En1^{Cre};mGFP* mouse embryos for the presence of phosphorylated histone H3 (pHH3), which is a marker for mitotic cells (A–D). Cells with a history of expressing *En1* as detected by the *mGFP* allele (nβ-gal+, red) were positioned in a DZ opposite to the VZ containing mitotic cells (green) of the dorsal Mb (A) and Cb (B). Faintly labeled pHH3+ cells (punctate green) were observed between these two zones (H, arrowheads). Mitotic cells (green) were distributed throughout the craniofacial region, which was devoid of *En1*-derived differentiated neurons (C). In contrast, the trigeminal ganglia were devoid of pHH3 labeling but had an abundance of differentiating neurons that had been derived from *En1* expressing cells (D). We analyzed *En1*-derived cells in the trigeminal ganglia from E12.5 embryos using the three different reporter alleles and compared marked cells to pHH3 (E–G). *En1^{Cre};mGFP* trigeminal contained marked cells (nβ-gal+, red) (E). *En1^{Cre};R26R* trigeminal also contained marked cells (β-gal+, red) (F). *En1^{Cre};Z/EG* trigeminal had *En1*-derived cells (GFP+, green). We did not detect pHH3 in the trigeminal ganglia with any of our marking schemes (E–G). We then compared marked cells and pHH3 in the dorsal Mb of *En1^{Cre}* mice and *Wnt1-CreER^{T}* mice with the different reporter alleles (H–L). Cumulative marking with *En1^{Cre};mGFP* showed that the *En1*-derived cells (red) were located in a zone opposite from pHH3+ mitotic cells in the VZ (green); the marked cells were never pHH3+(H). In contrast, *En1*-derived cells detected with the *Z/EG* reporter (GFP+, green) were distributed throughout the dorsal Mb including the superficial DZ and overlapped with pHH3+ cells (red) in the VZ (I, arrows). *En1^{Cre};R26R* Mb also had marked cells (β-gal+, red) in the DZ and the pHH3 + VZ (green) (J, arrows). GIFM with either *Wnt1-CreER^{T};mGFP* (K) or *Wnt1-CreER^{T};R26R* (L) revealed that the *mGFP* reporter labeled cells in the DZ (K, nβ-gal+, red), but not in mitotic cells (green) while the *R26R* reporter labeled cells (L, β-gal+, red) throughout the Mb including the DZ and the VZ (L, arrows). Thus, the *mGFP* reporter detects differentiated neurons while the *Z/EG* and *R26R* reporters label differentiated cells and mitotic progenitors. Arrow heads delineate pHH3+ cells located in between the VZ and DZ.

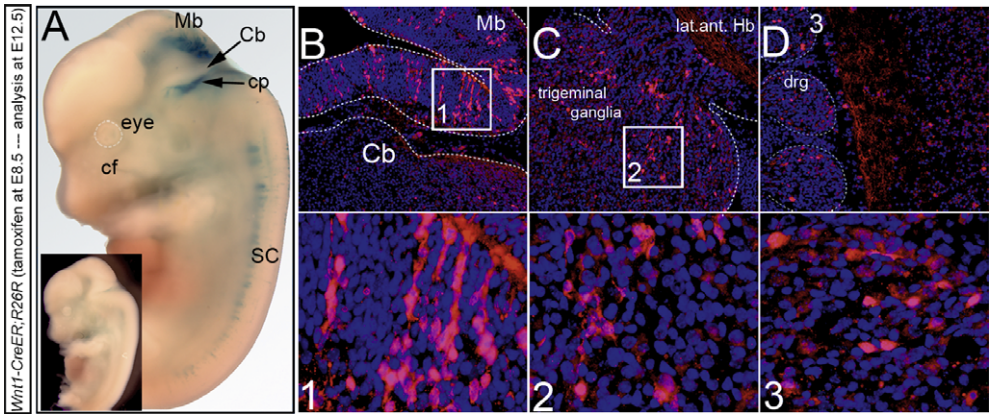

Fig. 7. GIFM of the *Wnt1* lineage in *Wnt1-CreER^{T};R26R* embryos. Tamoxifen was administered to pregnant females at E8.5 and embryos were assessed at E12.5 by whole-mount x-gal labeling (A) or by β-gal immunolabeling of sagittal sections (B–D). Fate mapped cells were observed in the Mb, choroid plexus (cp), and SC, but not in the Cb or body walls (A). In *R26R* littermates without the *Wnt1-CreER^{T}* transgene, no x-gal labeling was detected (A, inset). In off-midline sections (B), β-gal+ cells (red) were distributed as radially oriented "clonal-like" cohorts in the medial Mb (B-1). *Wnt1*-derived cells were not detected in the Cb (B). Marked cells of the trigeminal ganglia (C) were not organized into columns but were loosely distributed in the neuroepithelium (C-2). *Wnt1*-derived neurons in the SC were present in DRG (D, D-3).

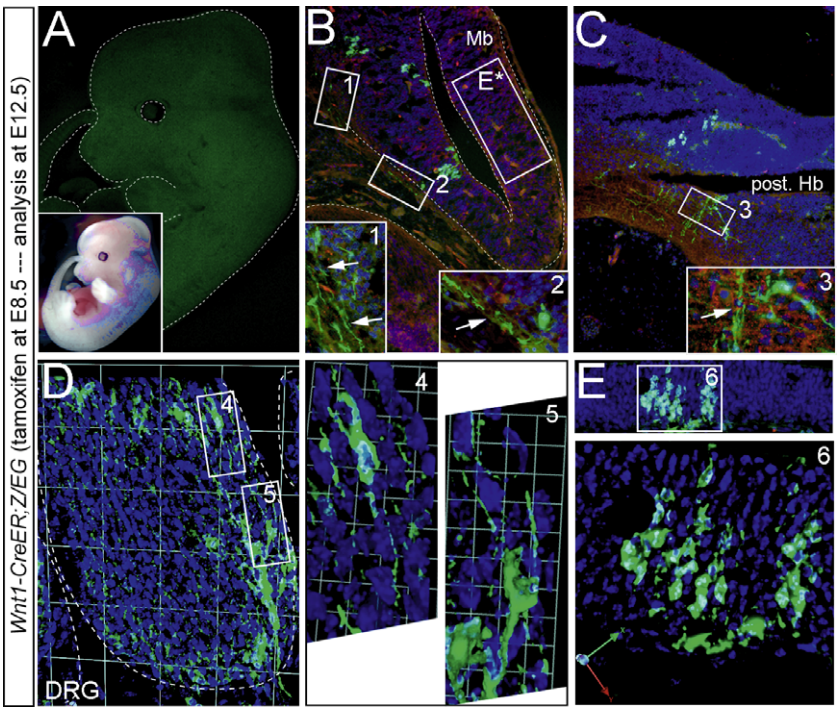

Fig. 8. GIFM of the *Wnt1* lineage with the *Z/EG* reporter allele. Tamoxifen administration at E8.5 did not yield appreciable labeling when analyzed by whole-mount fluorescence (A); a bright field image of the unlabeled embryo (A, inset). However, GFP immunolabeling on sections revealed a sparse population of marked cells (B,C). The location of the marked cells was consistent with *Wnt1-CreER^{T};R26R* and *Wnt1-CreER^{T};mGFP* embryos. In the lateral–dorsal Mb (B) small cohorts of cells were marked and displayed fine axonal projections (B-1, B-2, arrows). In the posterior Hb (post Hb), which is caudal to the Cb, the labeled neurons had projections that were localized to a cell-sparse zone (C) and displayed an elaborate morphology (C-3). The DRG (D) contained immature neurons with well-defined morphology (D-4, D-5) while the superior colliculus contained clusters of cell with immature morphology (E, E-6).

Interestingly, cohorts of *Wnt1*-derived neurons in the SC were distributed in DRG (Fig. 9K). Axons of these individually marked neurons exited the DRG forming thick bundles that passed between the rib cartilage and innervated the body wall (Fig. 9K). In contrast, cumulatively marked *En1*-expressing neurons (with *En1^{Cre};mGFP*) did not contribute to the DRG. This is interesting because the DRG and trigeminal ganglia are both comprised of bipolar neurons connected to the CNS and periphery, but the DRG is derived from *En1*(−)/*Wnt1*(+) precursors while the trigeminal ganglia is derived from *En1*(+)/*Wnt1(+)* progenitors. This report is the first that we are aware of describing the temporal nature of *Wnt1*-expressing cells contributing to DRG and complements previously published cumulative marking with *Wnt1-flipase* (Dymecki and Tomasiewicz, 1998).

In summary, β-gal and GFP double immunofluorescent labeling on sections from embryos marked using GIFM and the *mGFP* phenotyping allele provided an advantage over the *R26R* or *Z/EG* reporters because of flexibility and clarity. By comparing the *R26R*, *Z/EG* and *mGFP* reporters at E12.5 with both cumulative marking and GIFM paradigms, we observed that along with distinguishing between neural progenitors and differentiating neurons, we could more clearly follow axonal projections as they fasciculated or bifurcated and innervated distinct regions with the *mGFP* reporter line.

1.4. Neural projections and genetic lineage

Determining the developmental profile of axonal projection patterns and elucidating how neural circuits form both anatomically and physiologically is important in the context of brain development, neurological disease, and cell-based therapeutic approaches to ameliorate diseases of the nervous system. Numerous technical advances and genetic approaches have allowed for the examination of neural circuits. However, most of the methods in mouse models rely on recombinant viral technology (Morrow et al., 2008) or by genetically modifying an allele by inserting *Tau-LacZ* or *GFP* under the control of a specific gene such that manipulated cells and their circuits will be discernible (reviewed in Luo et al., 2008). It was previously suggested that Cre-mediated recombination concomitant with second-generation phenotyping alleles could uncover the logic of genetic neuroanatomy (Joyner and Zervas, 2006). Although GIFM has led to a deeper understanding of how cells expressing genes at distinct time points in development contribute to developing and mature structures (Kimmel et al., 2000; Zervas et al., 2004; Ahn and Joyner, 2005), experimental evidence relating specific lineages to developing neural circuits has not been ascertained.

Cumulative marking with *En1^{Cre}* and comparing *Z/EG* and *mGFP* phenotyping alleles demonstrated that the trigeminal ganglia contained *En1*-derived differentiated neurons (Fig. 5F) and was devoid of pHH3+ progenitor cells (Fig. 6E–G). Notably, GFP+ projections emanated from the differentiated neurons in the lateral anterior Hb and joined a complex plexus of axons. One portion of the plexus traversed along the anterior–posterior axis as a broad fascicle located interiorly within the ventral brain stem (Fig. 5E, arrows; Fig. 5F, bracket/arrow). The more peripheral axons fasciculated as a tight band that was parallel to the internal bundle (Fig. 5F, yellow arrowhead/small bracket). From the internal projections, axons bifurcated into columns that passed through the posterior half of the trigeminal ganglia (Fig. 5F, white arrowheads) and were directly connected to trigeminal neurons. In contrast, the anterior portion of the trigeminal ganglia had a thick conduit of axons that innervated the lateral craniofacial tissue including the vibrissae and three invariant points around the eye (Figs. 5F, 2J). Thus, *En1*-derived neurons formed a continuous network (lateral–anterior–dorsal Hb to trigeminal ganglia to craniofacial structures) that

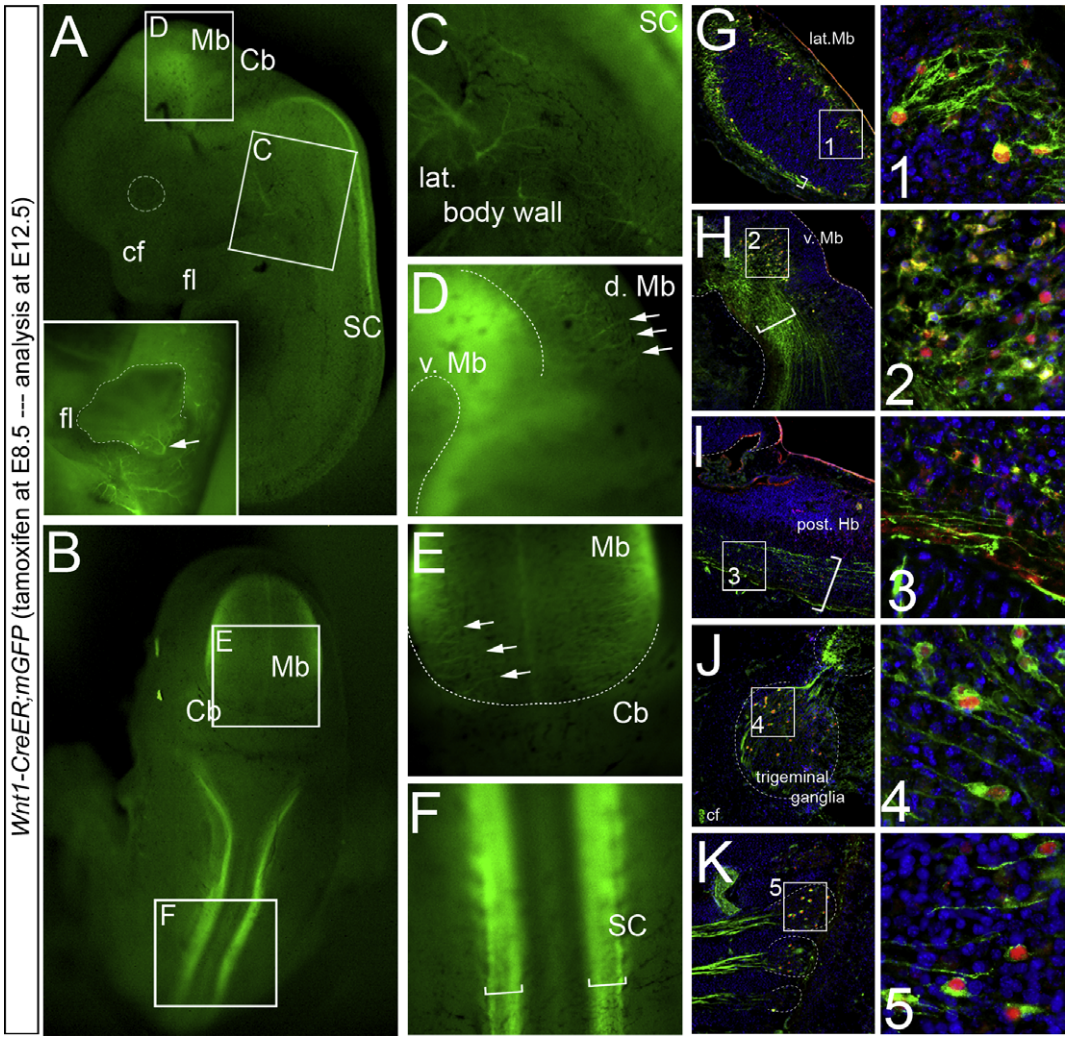

Fig. 9. GIFM of *Wnt1* derived neurons and developing neural circuits in E12.5 *Wnt1-CreER^T;mGFP* embryos. Tamoxifen was administered at E8.5 and *Wnt1-CreER^T;mGFP* embryos were analyzed four days later. Whole-mount GFP fluorescence was detected in the Mb, posterior Hb, and SC (A, B). Projections could be followed from the SC as they branched in the body wall (C) and innervated the forelimb (fl) (A, inset). A dense plexus located in the ventral Mb (D) is compared to evenly spaced radially oriented axonal branches in the dorsal Mb (D, E, arrows). In the SC region, the projections appeared more dorsal than those seen in *En1^{Cre};mGFP* embryos (F, brackets). Some of the projections may be Hb projections coursing in close proximity to the SC. In sagittal sections, neurons of the lateral–dorsal Mb (G) were located distal to the surface of the tissue but had elaborate morphology (G-1) with processes that spanned the outer 'shell' of the Mb and contacted the pial surface (G). In the ventral Mb (H) a cluster of β-gal+ cells (H-2, red) had projections that joined a thick fascicle running rostral-to-caudal in a zone distal to the ventricular zone (H, bracket). In the posterior Hb (I), projections were localized along the ventral half of the tissue (I-3). The projections connecting the lateral Hb and trigeminal ganglia (J) were readily discerned as were β-gal+ nuclei within the trigeminal ganglia (J). The neurons in the ganglia were largely bipolar (J-4). In the SC (K), neurons of the DRG were clearly marked (K-5) and had axons that traversed between intercostal domains innervating the lateral body wall (K, A, inset).

shared a common genetic background, being derived from *En1* expressing cells. Because the trigeminal ganglia does not have *En1* expressing cells at E12.5 as determined by *En1 in situ* hybridization (Supplemental Fig. 1F–J), the *En1*-derived cells were likely derived from earlier migrating neural crest cells.

The *Wnt1* lineage, marked by GIFM and tamoxifen administration at E8.5, showed that the trigeminal ganglia also consisted of differentiating neurons derived from *Wnt1* expressing progenitors (Fig. 10). The mosaic nature of GIFM was advantageous because we could clearly delineate neurons in the trigeminal ganglia, which revealed their bipolar morphology and axons that coalesced to form localized fascicles (Fig. 10A and B). Notably, the *Wnt1*-lineage contributed to the full extent of the trigeminal ganglia when temporally marked at E8.5. The *Wnt1*-derived projections on the posterior side of the trigeminal ganglia connected directly to the lateral Hb flexure (Fig. 10C and D) and were clustered into tight columns (Fig. 10C) that were then loosely connected with the Hb (Fig. 10D). *Wnt1*-derived neurons sparsely populated the inner portion of the Hb flexure (β-gal+) (Fig. 10E) and were positioned on the opposite side of the flexure (Fig. 10 reference, arrowheads) to where the *En1 (r1)*-derived neurons were observed. These *Wnt1*-derived neurons formed long sparse tangential projections of the inner plexus (Fig. 10E). The more peripheral, dense projections at the flexure appeared to be projections that connected with the trigeminal ganglia. *Wnt1*-derived trigeminal neurons innervated the craniofacial region and occasionally branched from the primary fascicle and terminated in 3-dimensional clusters (Fig. 10F) and innervated positions that were similar to the *En1*-derived connections around the eye, although there were fewer projections that joined the whisker pad vibrissae. High magnification of 1 μm thick optical sections and z-series acquisition demonstrated that the *mGFP* allele allowed for detailed analysis of single axons as they

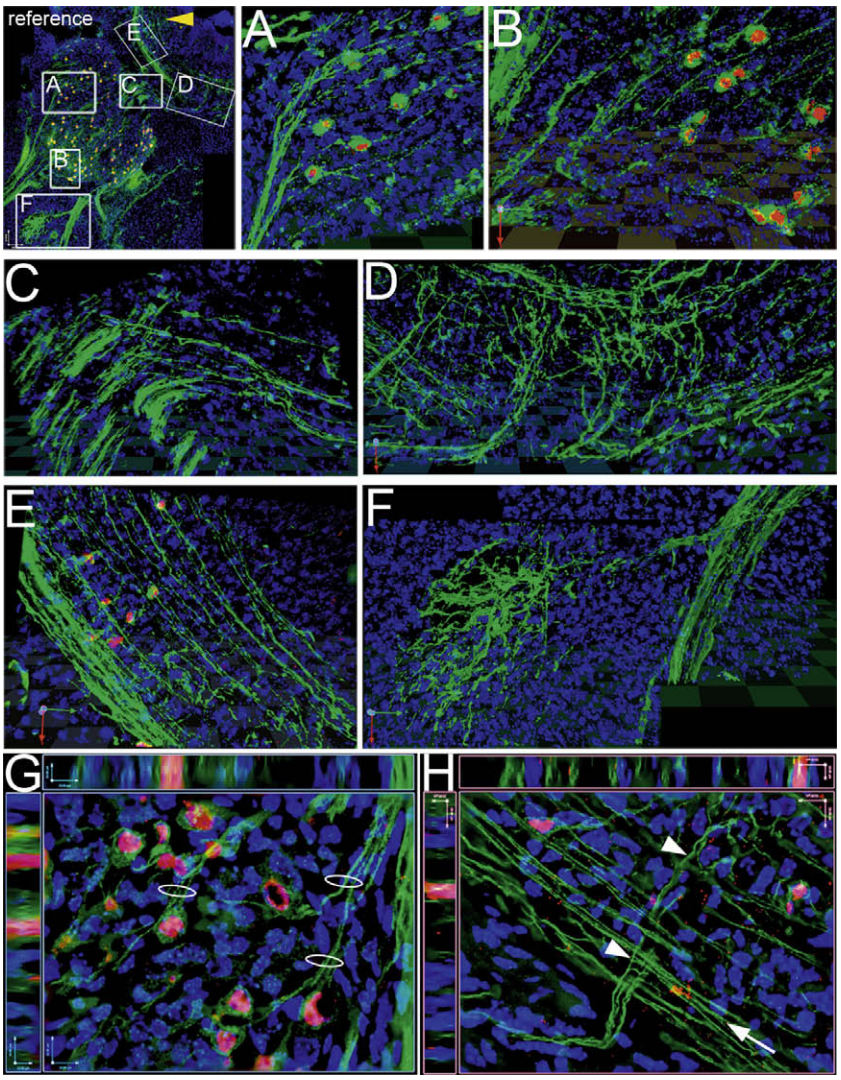

Fig. 10. *Wnt1*-derived neural circuits of the trigeminal ganglia. The reference panel (reference) shows the various regions that we sampled by z-series acquisition using 1μm thick optical planes followed by 3-D reconstructions. *Wnt1*-derived neurons (nβ-gal+, red) in the trigeminal had fine axons that formed fascicles, which emanated from the trigeminal and connected with the rostral craniofacial regions (A, B). At the pontine flexure fate mapped axons (GFP+, green) were organized into mini-columns radially organized and perpendicular to the axons located at the periphery of the pontine flexure (C). The axons within the pontine flexure were also organized into discrete units that primarily bifurcated at a more interior position and ramified in the interior stratified portion of the lateral Hb (D). Neuronal cell bodies marked within the lateral–posterior Hb tended to have long sparse tangential fibers that were uniformly aligned (E). Within the craniofacial domain, the *Wnt1*-derived neurons of the trigeminal often had a small number of axons that emanated from the main fascicle, arborized, and formed an elaborate plexus (F). High magnification microscopy of single optical sections allowed us to determine that single projections from trigeminal neurons tended to fasciculate with axons passing in close proximity to the site from where they extended; the rings show examples of points of fasciculation (G). The projections within the pontine flexure showed a complex arrangement: axons connected to the trigeminal (arrowheads) often passed over the longitudinally-oriented axons (arrowheads) (H).

came in close opposition to each other where they formed micro-columns in the trigeminal (Fig. 10G, ovals). Similarly, detailed analysis of the axons in the Hb flexure revealed that axons from the trigeminal tended to course over the longitudinally projecting axons and elaborated branches in the interior of the Hb (Fig. 10H).

In contrast, analysis of the SC and body wall revealed that *En1* and *Wnt1* derived neurons did not populate the same region of the cord nor did they form connections with common targets. *En1* is expressed in SC (Joyner and Martin, 1987; Davidson et al., 1988) and with $En1^{Cre}$ we confirmed that these cells contributed to the ventral SC as previously described (Saueressig et al., 1999). An advantage of the *mGFP* reporter was that we were able to observe marked cells by nuclear β-gal labeling and follow their axons with GFP, which showed that *En1*-derived cells are located in two bilateral columns in the SC with projections that radiate outward toward the periphery of the cord where they form a fascicle that exits the plane of the cord (Figs. 4 and 5G-3), which is in agreement with Saueressig et al. (1999). Adjacent to the cord a non-neural *En1*-derived domain was detected in the intercostal region of the body wall. In contrast, the *Wnt1* lineage marked at E8.5 contributed to DRG neurons. Thus, unlike the brainstem-trigeminal ganglia-craniofacial complex, *En1* and *Wnt1* lineages give rise to non-overlapping structures in the spinal cord. A novel finding ascertained by comparing $En1^{Cre}$;*Z/EG* or $En1^{Cre}$;*R26R* embryos in which the body wall is marked (Fig. 4G-3) with *Wnt1-CreER*^{T};*mGFP* embryos (Fig. 9K) is that *Wnt1*-derived DRG neurons (marked at E8.5) passed between *En1*-derived intercostal tissue and penetrated lateral–ventral tissue including the limbs (Fig. 9A; inset, 9C). In summary, using the *mGFP* phenotyping allele in cumulative marking versus GIFM we coupled genetic lineage to neural circuit formation during embryogenesis and suggest that this is a viable approach for reconstructing selectively marked circuits *in vivo*.

1.5. Assessment of the R26R, Z/EG, and mGFP phenotyping alleles at E10.0

We assessed embryos at E10.0 that had been marked either cumulatively or with GIFM to compare how the reporters behaved at two developmental stages (E10.0 and E12.5). For cumulative marking we compared *En1^{Cre};R26R*, *En1^{Cre};Z/EG*, *and En1^{Cre};mGFP* embryos (Supplemental Fig. 2A–C). For GIFM, we used *Wnt1-CreER^{T};R26R*, *Wnt1-CreER^{T};Z/EG*, and *Wnt1-CreER^{T};mGFP* embryos that had been subjected to tamoxifen at E8.5 and analysis 36 h later (Supplemental Fig. 2D–F). The *R26R* phenotyping allele produced marked cells, as detected with x-gal labeling, in both cumulatively and conditionally marked embryos (Supplemental Fig. 2A and D). The distribution of marked cells reliably labeled domains that are apparent precursors to the domains observed at E12.5. Comparatively, when using the *Z/EG* allele in conjunction with *En1^{Cre}* cumulative marking, cell somata and in the case of the nervous system, neuronal processes, could be readily detected in whole-mount embryos without tissue processing using a standard epi-fluorescent dissecting microscope (Supplemental Fig. 2B). The *Z/EG* phenotyping allele revealed cumulatively marked regions that appeared similar to domains detected with the *R26R* reporter including the mes and r1 as well as neural crest derivatives migrating into craniofacial regions and into the first branchial arch (Supplemental Fig. 2A and B). In sections of *En1^{Cre};Z/EG* embryos, cumulatively marked (GFP+) cells were easily detected in neural and non-neural tissue with neurons displaying clear morphological features including axonal projections (data not shown). Surprisingly, we did not detect any marked cells in *En1^{Cre};mGFP* embryos by whole-mount analysis at E10.0 (Supplemental Fig. 2C), although a relatively small number of differentiating neurons were observed in sections labeled with β-gal/GFP antibodies (data not shown). Of the three phenotyping alleles used in GIFM experiments in which tamoxifen was administered at E8.5, only the *R26R* reporter showed marking by whole-mount analysis at E10.0 (Supplemental Fig. 2D–F). Thus, cumulative marking or temporal GIFM of genetic lineages with the *R26R* allele allows for the detection of cell somata with minimal tissue processing in whole-mount embryos. In sections, β-gal+ cells were readily detected in E10.0 *Wnt1-CreER^{T};R26R* embryos (Zervas et al., 2004). In contrast, a small amount of differentiating GFP + cells could be detected in sections from E10.0 *Wnt1-CreER^{T};mGFP* embryos, but no marked cells were observed in E10.0 *Wnt1-CreER^{T};Z/EG* embryos (data not shown). However, when these alleles were used with *Wnt1-CreER^{T}* and marked at the same time point (E8.5), temporally marked cells could be detected at E12.5 in whole-mount embryos and in sections. These findings suggest that at E10.0 there are very few differentiated neurons, which are only detectable by antibody-enhanced labeling, but not by whole-mount fluorescent detection. The reason for the lack of marking with the *Z/EG* reporter in GIFM experiments at E10.0 may be that the EGFP from the *Z/EG* allele requires a sufficient amount of time to be produced and accumulate in cells. This is an important consideration in GIFM experiments where the ascertainment of morphogenetic movements is desired. In particular, use of the *Z/EG* allele in conditional marking experiments may preclude the ability to determine of the distribution of the initially marked population prior to subsequent movements (reviewed in Joyner and Zervas, 2006).

1.6. Assessment of the Z/EG, and mGFP phenotyping alleles in the adult brain

The use of appropriate phenotyping alleles provided excellent details of developing cell populations. We also determined their value in understanding how progenitor cells transiently expressing genes contribute to complex anatomical and functional structures in the adult brain (Supplemental Fig. 3). Tamoxifen administration at E8.5 resulted in marking of cells distributed in the dorsal Mb of the adult consistent with previous findings using the *R26R* reporter (Zervas et al., 2004). We focused on the GFP phenotyping alleles because of their putative ability to delineate cell morphology and axonal projections. The *Z/EG* and *mGFP* phenotyping alleles yielded similarly marked spatial domains (for example the dorsal Mb), but marked cells in the *Wnt1-CreER^{T};Z/EG* background were far more sparse than observed with the *Wnt1-CreER^{T};mGFP* line (Supplemental Fig. 3A and B). The *Z/EG* line provided clear morphological details and cellular resolution with GFP immunolabeling, for example revealing processes emanating from neuronal somata (Supplemental Fig. 3A, inset). In contrast, the *mGFP* line revealed a rich plexus of projections (GFP+) and β-gal+ nuclei (Supplemental Fig. 3B, inset), which may be useful in combination with marker analysis. Close inspection of double immunolabeled neurons in *Wnt1-CreER^{T};mGFP* mice revealed that GFP was faintly localized to neuronal somata as opposed to intensely labeled projections (Supplemental Fig. 3B, inset). We also administered tamoxifen to *Wnt1-CreER^{T};Z/EG* and *Wnt1-CreER^{T};mGFP* embryos at E11.5, when *Wnt1* expression has become more restricted and substantially marks the posterior Hb (Zervas et al., 2004). Neurons had well-discernible morphological features when GFP antibody labeling was used with the *Z/EG* phenotyping allele (Supplemental Fig. 3C). The *mGFP* reporter yielded more marked cell nuclei and discrete projections, as observed with β-gal/GFP double immunolabeling (Supplemental Fig. 3D) when compared to the same domain in the *Z/EG* line. Finally, we examined cumulative marking in the posterior Hb of adult *En1^{Cre};Z/EG* mice (Supplemental Fig. 3E) to maximize the number of cells expressing the *Z/EG* reporter. We observed numerous morphologically distinct neurons including calretinin-positive neurons (Supplemental Fig. 3E, arrows) and could also detect fine axonal projections oriented longitudinally in the posterior Hb. With *Wnt1-CreER$^{T;}$mGFP* marking, we also observed substantial marking in the posterior Hb, but could not clearly discriminate neuronal morphology (Supplemental Fig. 3F).

In summary, we used cumulative marking and GIFM with three different reporter alleles and ascertained the strengths of each phenotyping allele in a comparative analysis (Table 1). Each of these reporters provides a robust view of developmental biology and uncovered unique features related to lineage and development. We demonstrate that when used comparatively, the three reporters provide a very detailed analysis of marked cells and axonal projections. This was exemplified in both cumulative marking and GIFM approaches. Notably, we also have gained a further understanding of the overlapping and complementary contribution of *En1* and *Wnt1* expressing cells to both neural and non-neural tissue over time. The information provided here is likely to be valuable to the developmental biology and neurobiology community to help elucidate which allele is most applicable to specific biologically relevant questions.

2. Experimental procedures

2.1. Mice

The generation of *Wnt1-CreER^{T}* and *En1^{Cre}* mice were previously described (Zervas et al., 2004; Kimmel et al., 2000). The *R26R* reporter mice were generously provided by P. Soriano (Soriano, 1999), the *Z/EG* mice (Novak et al., 2000) were obtained from Jackson Laboratories (stock # 003920), and *Tau^{mGFP}* (*lox-STOP-lox-mGFP-IRES-NLS-LacZ-pA*) mice (Hippenmeyer et al., 2005) were generously provided by S. Arber. Mice were housed and handled in accordance with Brown University Institutional Animal Care and Use Committee guidelines.

Table 1
Summary of cumulative marking and GIFM results at E12.5. The regions described in the text using *En1^{Cre}* (cumulative marking) and *Wnt1-CreER* (GIFM) are summarized with an emphasis on proliferating and differentiating cells as defined by pHH3 labeling. The figures showing the results are also indicated. (√), detected; (–), not detected; nd, not determined.

Line	Region	Proliferating cells	Differentiating neurons	Figure reference
En1^{Cre};R26R	Mb	√	√	3A, 3B, 6J
	Cb	√	√	3A, 3B
	Lat Hb	√	√	3E
	Trigeminal	–	√	3E, 6F
	v. SC	nd	nd	ns
	DRG	–	–	ns
En1^{Cre};Z/EG	Mb	√	√	4A, 4B, 4G, 6I
	Cb	√	√	4A, 4B
	Lat Hb	√	√	4E, 4F
	Trigeminal	–	√	4E, 4F, 6G
	v. SC	nd	√	4G-3
	DRG	–	–	4G-3
En1^{Cre};mGFP	Mb	–	√	5A, 5B, 6A, 6H
	Cb	–	√	5A, 5B, 6B
	Lat Hb	–	√	5E, 5F
	Trigeminal	–	√	5E, 5F, 6D, 6E
	v. SC	nd	√	5G-3
	DRG	–	–	5G-3
Wnt1-CreER^{T};R26R	Mb	√	√	7B, 6L
	Cb	–	–	7B
	Lat Hb	√	√	ns
	Trigeminal	–	√	7C
	v. SC	–	–	ns
	DRG	nd	√	7D
Wnt1-CreER^{T};Z/EG	Mb	√	√	8B, 8E
	Cb	–	–	ns
	Lat Hb	√	√	8C
	Trigeminal	nd	nd	ns
	v. SC	–	–	ns
	DRG	nd	√	8D
Wnt1-CreER^{T};mGFP	Mb	–	√	9D, 9E, 9G, 9H
	Cb	–	–	9E
	Lat Hb	–	√	10E
	Trigeminal	–	√	9J, 10A, 10B, 10G
	v. SC	–	–	ns
	DRG	–	√	9F, 9K

2.2. Genotyping

Embryonic tail was digested in 100 μL of tail lysis buffer (containing Proteinase K) for 12 h at 60 °C followed by heat activation at 90 °C for 10 min. A 600 bp fragment of Cre or CreER was amplified in a 20 μL reaction (16.54 μL of ddH_2O, 2 μL of 15 mM $MgCl_2$ 10× buffer, 0.16 μL of 100 mM dNTPs (25 mM each nucleotide), 0.10 μL each of 150 pmol/μL NLS-Cre forward primer (5′-TAA AGA TAT CTC ACG TAC TGA CGG TG-3′) and 150 pmol/μL NLS-Cre reverse primer (5′-TCT CTG ACC AGA GTC ATC CTT AGC-3′), 0.10 μL of Taq enzyme (Invitrogen; Carlsbad, CA) and 1.0 μL of tail lysate DNA template] using a Eppendorf PCR cycler (94 °C for 2 min, 30 cycles of 94 °C for 30 s, 58 °C for 1 min and 72 °C for 30 s, and 72 °C for 10 min). A 250 bp fragment of the *R26R* allele was amplified in a 20 μL reaction [12.44 μL of ddH_2O, 2 μL of 15 mM $MgCl_2$ 10× buffer, 0.16 μL of 100 mM dNTPs, 0.10 μL of 150 pmol/μL *R26R* primer 1 (5′-GCG AAG AGT TTG TCC TCA ACC-3′), 0.10 μL of 150 pmol/μL *R26R* primer 2 (5′-GCG AAG AGT TTG TCC TCA ACC-3′), 0.10 μL of 150 pmol/μL *R26R* primer 3 (5′-GGA GCG GGA GAA ATG GAT ATG-3′), 0.10 μL of Taq enzyme and 5.0 μL of tail lysate DNA template] with the following PCR program (94 °C for 2 min, 30 cycles of 94 °C for 1 min, 64 °C for 1 min and 72 °C for 1 min, and 72 °C for 10 min). A 600 bp amplicon indicating the *mGFP* or *Z/EG* allele was amplified in a 20 μL reaction [15.54 μL of ddH_2O, 1 μL of DMSO, 2 μL of 15 mM $MgCl_2$ 10× buffer, 0.16 μL of 100 mM dNTPs, 0.10 μL of 150 pmol/μL *EGFP* sense primer (5′-CTG GTC GAG CTG GAC GGC GAC G-3′), 0.10 μL of 150 pmol/μL *EGFP* anti-sense primer (5′-CAC GAA CTC CAG CAG GAC CAT G-3′), 0.1 μL of Taq enzyme and 1.0 μL of tail lysate DNA template] using the following PCR program (94 °C for 3 min, 30 cycles of 94 °C for 30 s, 60 °C for 30 s and 72 °C for 1 min, and 72 °C for 3 min). About 4 μL of 6× loading dye was added to the PCR products and heated to 65 °C for 5 min. Samples were then run on a 2% agarose gel containing SYBRsafe (Invitrogen, S33102 at a concentration of 1 μl/100 mL in TBE) at 140 V for 1 h. Gels were visualized using a blue light box.

2.3. Fate mapping

A 20-mg/ml stock solution of tamoxifen (T-5648, Sigma) was prepared by dissolving tamoxifen in pre-warmed corn oil (C-8267 Sigma) followed by intermittent vortexing during a 2-h incubation on a ** nutator at 37 °C. The tamoxifen stock was protected from light, stored at 4 °C, and used for a one month duration. Fate mapping experiments were conducted by crossing *Wnt1-CreER^{T};R26R*, *Wnt1-CreER^{T};Z/EG*, *Wnt1-CreER^{T};mGFP* male mice with Swiss Webster (SW, wildtype; purchased from Taconic) female mice. The morning (0900) of the day a vaginal plug was detected was designated as 0.5 days post-coitus. Tamoxifen was administered at a dose of 4 mg (200 μl) to time-pregnant SW females by oral gavage at 0900 h. Mice were sacrificed according to Brown University Institutional Animal Care and Use Committee guidelines at described experimental time points. Mouse embryos (minimally, $n \geqslant 3$ embryos across two or more litters) were dissected

free, genotyped, and processed for whole-mount or x-gal labeling, ISH, or were cryoprotected for tissue and cellular analysis.

2.4. Whole-mount β-galactosidase histochemistry and in situ hybridization (ISH)

Embryos were fixed with 4% paraformaldehyde (PFA) for 20 min at room temperature (RT), rinsed in PBS, and incubated twice (10 min/each) in x-gal wash buffer (2 mM $MgCl_2$, 0.1% Igepal Ca-30, 0.05% deoxycholate in PBS). Subsequently, *Wnt1-CreER^T;R26R* embryos were incubated overnight at 37 °C in x-gal reaction buffer [0.106 g potassium ferrocyanide, 0.082 g potassium ferricyanide, 48 ml of x-gal wash buffer and 2 ml of x-gal substrate stock solution (25 mg x-gal/ml in DMSO)]. For *En1^{Cre};R26R* embryos, a shorter processing time (4 h) was also used because we observed that the marked expression domains became so thoroughly labeled that the blue reaction product obscured detailed tissue analysis. For whole-mount RNA ISH, embryos were fixed in PFA overnight at 4 °C, and subsequently washed in PBS, SSC, and hybridization buffer at 60 °C for 2–3 h, and hybridized with digoxigenin (dig)-labeled RNA probes (1–2 μl) in 500 μl hybridization buffer. Embryos were washed with high stringency buffers, blocked in embryo powder/NGS/PBS, and processed for alkaline phosphatase (AP)-conjugated anti-dig antibody (Roche) over night at 4 °C. The next day embryos were washed with NTMT and incubated in AP substrate (BM purple) in NTMT-levamisole until the desired color reaction was achieved.

2.5. Tissue processing and cryosectioning

Embryos identified for tissue/cellular analysis were dissected in PBS over ice and a small (1–2 mm) tail sample was obtained for genotyping. Embryos were fixed in 4% PFA for 4 h to overnight at 4 °C. Subsequently, embryos were rinsed in PBS and immersed in 15% sucrose and 30% sucrose until submerged. We removed the sucrose and equilibrated the embryos briefly in Optimal Cutting Temperature (OCT) followed by orienting and embedding embryos in OCT in cryomolds. Subsequently embryos were immersed in 2-methyl-butane as described (http://www.adam.com.au/royellis/fr.htm). Briefly, 2-methyl butane is placed in a polypropylene beaker, which is carefully placed in an appropriate vessel to hold liquid nitrogen. Once the temperature reaches −150°C, the specimen is placed into the cooled 2-methyl-butane until frozen. Samples were stored in sealed bags at −20°C. Sections were obtained on a Leica cryostat and mounted on Fisher Biotech Probe On Plus slides (No. 15-188-52).

2.6. Section ISH

Cryosections (12 μm) were obtained and stored at −20°C until thawed for use. Sections were fixed in 4% paraformaldehyde (PFA) in PBS for 10 min, then washed with PBS two times for 5 min each. Slides were incubated in 2 μg/mL proteinase K in PBS for 4 min, washed with PBS for 5 min, re-fixed in 4% PFA for 5 min and washed in PBS four times for 5 min each. Slides were dehydrated in 70% EtOH for 5 min and in 95% EtOH for approximately 2 min and allowed to air dry slightly. The appropriate *in situ* probe and hybridization solution were combined at a concentration of 2 μL/mL and heated at 80 °C for 2 min. We generated a *Cre* probe by sub-cloning a 1 kb fragment of *Cre* into pKS plasmid. The anti-sense *in situ* probe was generated by NotI digest and digoxigenin-nucleotide labeling with T3 polymerase; 4 μL/mL of probe was added to hybridization buffer. For *En1*, we digested a plasmid with ClaI and used T7 polymerase and for *Wnt1*, we digested a plasmid with ClaI and used SP6 polymerase. Slides were placed in a hyboven cassette containing autoclaved ddH_2O. Probe-containing hybridization solution (300 μL) was added to each slide and coverslipped with RNAse-free Hybridslips; samples were hybridized overnight at 55 °C. Coverslips were floated off using pre-warmed 5× SSC and slides were washed as follows: pre-warmed high stringency wash 1 time for 30 min at 65°, RNase buffer warmed to 37 °C 3 times for 10 min each, pre-warmed RNase buffer treated with 20 μg/mL of RNase A at 37 °C for 30 min, pre-warmed RNase buffer 1 time for 15 min, pre-warmed high stringency wash 2 times at 65 °C for 20 min each, pre-warmed 2× SSC at 37 °C for 15 min, 0.1× SSC at 37 °C for 15 min, and 0.1% Tween-20 in PBS (PBTween) for 15 min at room temperature. Slides were then placed in a humid box and blocked with 300 μL of 10% heat inactivated goat serum in PBTween at room temperature for 1 h and coverslipped with parafilm. Blocking solution was removed and slides were incubated overnight at 4 °C in alkaline phosphatase-coupled anti-digoxigenin antibody diluted 1:5000 in PBT with 1% goat serum and coverslipped with parafilm. The next day, slides were washed 4 times in PBTween at room temperature for 15 min each, then in NTMT buffer containing 0.5 mg/mL levamisole (Sigma; St. Louis, MO) 2 times for 10 min each. Gene expression domains were detected by staining slides with 0.5 mg/mL levamisole in BM Purple AP substrate (Roche; Indianapolis, IN) at room temperature overnight. Once development was complete (determined empirically) slides were washed in PBS for 5 min, post-fixed with 4% PFA for 2 min and washed in PBS for another 5 min. Sections were then counter-stained by incubations in water (1 min), Fast Red (Poly Scientific; Bay Shore, NY) for 3 min, water (1 min), 70% EtOH (1 min), 95% EtOH 2 times (1 min each), 100% EtOH 2 times (1 min each), and xylene 3 times (1 min each). Slides were allowed to air dry slightly and were then coverslipped using Permount (Fisher Scientific).

2.7. Immunocytochemistry

Cryosections (12 μm) were rinsed in PBS for 5 min and fixed in 4% PFA in PBS for 5 min. Slides were then rinsed 3 times in 0.2% TritonX-100 (Fisher Scientific; Waltham, MA) in PBS (PBT) for 5 min each and blocked in 10% donkey serum in PBT for 2 h at room temperature in a humid box. Anti-β-gal primary antibody (Biogenesis; Sultan, WA; Cat# 4600-1409; donkey anti-goat IgG) was prepared at 1:500 in 10% donkey serum in PBT and was used on all slides. Anti-TH primary antibody (Chemicon; Billerica, MA; Cat# AB152; Lot # 0603025098 donkey anti-rabbit IgG) or Anti-CALRET primary antibody (Chemicon; Billerica, MA; Cat# AB1550; donkey anti-rabbit IgG) was prepared at 1:500 in 10% donkey serum in PBT. Anti-EGFP primary antibody (Molecular Probes; Carlsbad, CA; Cat# A-11122; donkey anti-rabbit IgG) was prepared at 1:600 in 10% donkey serum in PBT and was used on all sections positive for the *mGFP* and *Z/EG* alleles. Anti-phospho-histone H3 (Ser10) antibody (Millipore; Temecula, CA; Cat #06-570; donkey anti-rabbit IgG) was prepared at 1:200 in 10% donkey serum in PBT and was used to distinguish mitotic cells. Slides were incubated in 300 μL of primary antibody solution at 4 °C in a humid box with a parafilm coverslip overnight. Slides were allowed to come to room temperature, coverslips were removed, and slides were washed 5 times with PBT for 10 min each. Alexa 555 secondary antibody (Molecular Probes; Cat # A-21432; donkey anti-goat IgG) and Alexa 488 secondary antibody (Molecular Probes; Cat # A-21206; donkey anti-rabbit IgG) were prepared at a concentration of 1:500 in 1% donkey serum in PBT. Sections were incubated in 300 μL of secondary antibody solution for 2 h at room temperature in a humid box with parafilm coverslips. Slides were then washed with PBT 5 times for 10 min each and counterstained with .01% Hoechst 33342 (Molecular Probes; Cat # H-3570) in PBS for 5 min in the dark. Slides were washed 2 times with PBS for 2 min each, dried and coverslipped.

2.8. Microscopy

Whole-mount fluorescence and x-gal processed embryos were obtained on a Leica MZ16F stereo fluorescent dissecting microscope using PictureFrame software. Images of sections were obtained on a Leica DM600B epifluorescent microscope with a 2.5× objective (low magnification images). High magnification images were obtained using a motorized stage with a 20× or 40× objective to collect 1 μm optical sections (in the *z*-axis), which were then analyzed with the Volocity 5.1 visualization module. All images were pseudo colored live as part of the acquisition palettes. 3-dimensional renderings of neurons shown in Figs. 8D–E, 10C–F were generated in the 3-dimension module of Volocity 5.1 using the entire z-stack of 1 μm optical sections followed by adjusting the density, brightness and contrast. It should be noted that the gamma values for 3D rendering were adjusted from the standard value of 1.0. However, the gamma value was unadjusted for all other data processing. Imaging data sets were exported to Adobe Photoshop CS2 or Adobe Illustrator CS2 where montages of representative data were generated.

Acknowledgements

We are grateful to S. Arber for the *mGFP* mice and to members of the Zervas lab who critically read the paper and provided technical assistance. N. Hagan was supported by an NINDS training grant (1T32NS062443, Brown University Department of Neuroscience) and by a Brain Science Program Graduate Research Award, through the Brain Science Program Reisman Fund. This research was also funded by startup research funds (MZ).

Appendix A. Supplementary data

Supplementary data associated with this article can be found, in the online version, at doi:10.1016/j.gep.2009.07.007.

References

Ahn, S., Joyner, A.L., 2004. Dynamic changes in the response of cells to positive hedgehog signaling during mouse limb patterning. Cell 118, 505–516.

Ahn, S., Joyner, A.L., 2005. In vivo analysis of quiescent adult neural stem cells responding to Sonic hedgehog. Nature 437, 894–897.

Aronov, S., Aranda, G., Behar, L., Ginzburg, I., 2001. Axonal tau mRNA localization coincides with tau protein in living neuronal cells and depends on axonal targeting signal. J. Neurosci. 21, 6577–6587.

Davidson, D., Graham, E., Sime, C., Hill, R., 1988. A gene with sequence similarity to *Drosophila* engrailed is expressed during the development of the neural tube and vertebrae in the mouse. Development 104, 305–316.

Dymecki, S.M., Kim, J.C., 2007. Molecular neuroanatomy's "Three Gs": a primer. Neuron 54, 17–34.

Dymecki, S.M., Tomasiewicz, H., 1998. Using Flp-recombinase to characterize expansion of Wnt1-expressing neural progenitors in the mouse. Dev. Biol. 201, 57–65.

Feil, R., Brocard, J., Mascrez, B., LeMeur, M., Metzger, D., Chambon, P., 1996. Ligand-activated site-specific recombination in mice. Proc. Natl. Acad. Sci. USA 93, 10887–10890.

Guo, C., Yang, W., Lobe, C.G., 2002. A Cre recombinase transgene with mosaic, widespread tamoxifen-inducible action. Genesis 32, 8–18.

Guo, Q., Loomis, C., Joyner, A.L., 2003. Fate map of mouse ventral limb ectoderm and the apical ectodermal ridge. Dev. Biol. 264, 166–178.

Hashimoto, Y., Muramatsu, K., Uemura, T., Harada, R., Sato, T., Okamoto, K., Harada, A., 2008. Neuron-specific and inducible recombination by Cre recombinase in the mouse. Neuroreport 19, 621–624.

Hayashi, S., McMahon, A.P., 2002. Efficient recombination in diverse tissues by a tamoxifen-inducible form of Cre: a tool for temporally regulated gene activation/inactivation in the mouse. Dev. Biol. 244, 305–318.

Hippenmeyer, S., Vrieseling, E., Sigrist, M., Portmann, T., Laengle, C., Ladle, D.R., Arber, S., 2005. A developmental switch in the response of DRG neurons to ETS transcription factor signaling. PLoS Biol. 3, e159.

Joyner, A.L., Martin, G.R., 1987. En-1 and En-2, two mouse genes with sequence homology to the *Drosophila* engrailed gene: expression during embryogenesis. Genes Dev. 1, 29–38.

Joyner, A.L., Zervas, M., 2006. Genetic inducible fate mapping in mouse: establishing genetic lineages and defining genetic neuroanatomy in the nervous system. Dev. Dyn. 235, 2376–2385.

Kimmel, R.A., Turnbull, D.H., Blanquet, V., Wurst, W., Loomis, C.A., Joyner, A.L., 2000. Two lineage boundaries coordinate vertebrate apical ectodermal ridge formation. Genes Dev. 14, 1377–1389.

Luo, L., Callaway, E.M., Svoboda, K., 2008. Genetic dissection of neural circuits. Neuron 57, 634–660.

Morrow, E.M., Chen, C.M., Cepko, C.L., 2008. Temporal order of bipolar cell genesis in the neural retina. Neural Dev. 3, 2.

Novak, A., Guo, C., Yang, W., Nagy, A., Lobe, C.G., 2000. Z/EG, a double reporter mouse line that expresses enhanced green fluorescent protein upon Cre-mediated excision. Genesis 28, 147–155.

Paxinos, G. (Ed.), 2004. The Rat Nervous System, third ed. Elsevier/Academic Press, Amsterdam; Boston. ISBN 0125476388.

Robinson, S.P., Langan-Fahey, S.M., Johnson, D.A., Jordan, V.C., 1991. Metabolites, pharmacodynamics, and pharmacokinetics of tamoxifen in rats and mice compared to the breast cancer patient. Drug Metab. Dispos. 19, 36–43.

Saueressig, H., Burrill, J., Goulding, M., 1999. Engrailed-1 and netrin-1 regulate axon pathfinding by association interneurons that project to motor neurons. Development 126, 4201–4212.

Soriano, P., 1999. Generalized lacZ expression with the ROSA26 Cre reporter strain. Nat Genet. 21, 70–71.

Wilkinson, D.G., Bailes, J.A., McMahon, A.P., 1987. Expression of the proto-oncogene int-1 is restricted to specific neural cells in the developing mouse embryo. Cell 50, 79–88.

Zervas, M., Blaess, S., Joyner, A.L., 2005. Classical embryological studies and modern genetic analysis of midbrain and cerebellum development. Curr. Top Dev. Biol. 69, 101–138.

Zervas, M., Millet, S., Ahn, S., Joyner, A.L., 2004. Cell behaviors and genetic lineages of the mesencephalon and rhombomere 1. Neuron 43, 345–357.

Zinyk, D.L., Mercer, E.H., Harris, E., Anderson, D.J., Joyner, A.L., 1998. Fate mapping of the mouse midbrain–hindbrain constriction using a site-specific recombination system. Curr. Biol. 8, 665–668.